JACC: BASIC TO TRANSLATIONAL SCIENCE VOL. 8, NO. 6, 2023

ORIGINAL RESEARCH - PRECLINICAL

RNA m^{6}A-Regulated *circ-ZNF609* Suppression Ameliorates Doxorubicin-Induced Cardiotoxicity by Upregulating FTO

Pujiao Yu, MD, PhD,[a,b,c,*] Jiaqi Wang, BA,[a,d,*] Gui-e Xu, BA,[a,d,*] Xuan Zhao, BA,[a,d,*] Xinxin Cui, MS,[a,d] Jingyi Feng, MS,[a,d] Jiangpeng Sun, BA,[a,d] Tianhui Wang, PhD,[a,d] Michail Spanos, PhD,[e] Helge Immo Lehmann, MD, PhD,[e] Guoping Li, PhD,[e] Jiahong Xu, MD, PhD,[b,c] Lijun Wang, PhD,[a,d] Junjie Xiao, MD, PhD[a,d]

VISUAL ABSTRACT

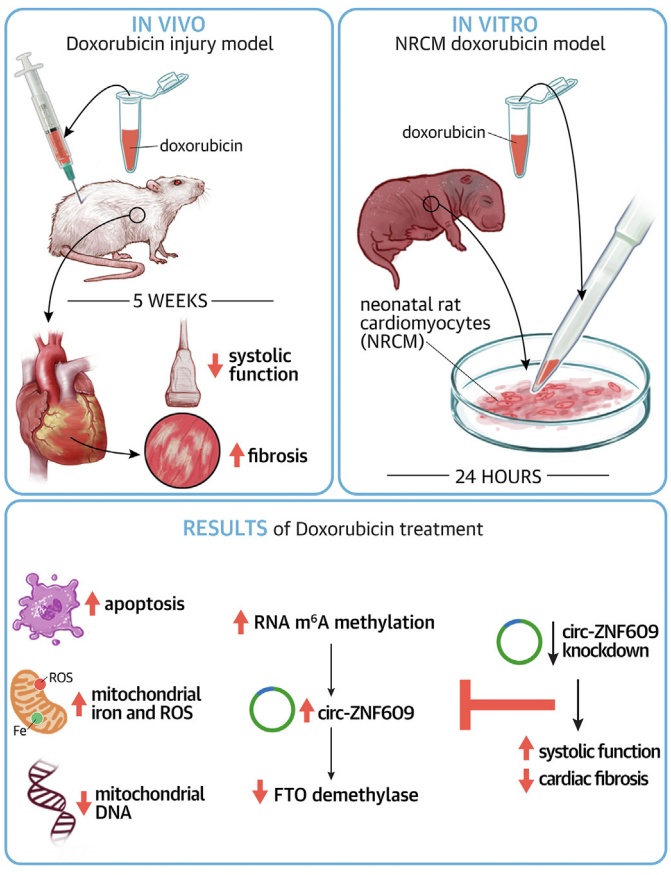

Yu P, et al. J Am Coll Cardiol Basic Trans Science. 2023;8(6):677-698.

HIGHLIGHTS

- **Cardiac death is a major burden for cancer survivors, yet there is currently no effective treatment for DOX-induced cardiotoxicity.**
- **circ-ZNF609 knockdown alleviates DOX-induced cardiotoxicity through attenuating cardiomyocyte apoptosis, reducing ROS production, ameliorating the mitochondrial nonheme iron overload.**
- **circ-ZNF609 inhibition blocks the elevation effect of RNA m^{6}A methylation level in mice hearts by DOX treatment, whereas RNA m^{6}A demethylase FTO acts as the downstream factor of circ-ZNF609.**
- **Therapeutics targeting circ-ZNF609 might be a potential novel strategy for attenuating DOX-induced cardiotoxicity.**

ISSN 2452-302X https://doi.org/10.1016/j.jacbts.2022.12.005

JACC: BASIC TO TRANSLATIONAL SCIENCE VOL. 8, NO. 6, 2023
JUNE 2023:677–698

ABBREVIATIONS AND ACRONYMS

DOX = doxorubicin

circRNA = circular RNA

FTO = fat mass and obesity associated gene

METTL14 = methyltransferase like 14

mtDNA = mitochondria DNA

NRCM = neonatal rat cardiomyocyte

RNA m^{6}A = RNA N^6-methyladenosine

ROS = reactive oxygen species

ZNF609 = zinc finger protein 609

SUMMARY

Cardiac death is a major burden for cancer survivors, yet there is currently no effective treatment for doxorubicin (DOX)-induced cardiotoxicity. Here, we report that circ-ZNF609 knockdown knockdown had cardioprotective effects against DOX-induced cardiomyocyte toxicity. Mechanistically, circ-ZNF609 knockdown alleviated DOX-induced cardiotoxicity through attenuating cardiomyocyte apoptosis, reducing reactive oxygen species production, ameliorating mitochondrial nonheme iron overload. circ-ZNF609 inhibition blocked the elevation of RNA N^6-methyladenosine (RNA m^{6}A) methylation level in DOX-treated mice hearts, whereas m^{6}A demethylase fat mass and obesity associated (FTO) acted as the downstream factor of circ-ZNF609. Moreover, the stability of circ-ZNF609 was regulated by RNA m^{6}A methylation alteration, and suppression of RNA m^{6}A methylation by methyltransferase like 14 (METTL14) modulated the function of circ-ZNF609. These data suggest that circ-ZNF609 inhibition represents a potential therapy for DOX-induced cardiotoxicity.

Despite modern chemotherapeutic protocols that have greatly prolonged the 5-year survival rate of cancer patients, their side effects on nontargeted tissues are still severely compromising long-term prognosis of those patients as a double-edged sword.[1] Doxorubicin (DOX) is one of the most widely used anthracycline chemotherapeutic agents despite its extensive adverse event profile.[2] It is now well established that the cardiotoxicity resulting from chemotherapy poses a significant risk for morbidity and mortality to the treated patient.[3] Several potential mechanisms responsible for DOX-induced cardiotoxicity have been revealed in past decades, including production of reactive oxygen species (ROS), damage of mitochondria DNA, and cardiomyocytes death.[4-8] However, there are still no preventative or curative strategies against DOX-induced cardiotoxicity.

Circular RNAs (circRNAs) represent a new class of noncoding RNAs that are generated by back-splicing.[9] Moreover, circRNAs play important regulatory roles in physiological or pathological processes.[10] Recently, we reported that circRNA circ-ZNF609 inhibition could protect against cardiac ischemia/reperfusion injury.[11] circ-ZNF609, also as known as myocardial infarction associated circular RNA, was reported early to be highly associated with myocardial infarction prognosis.[12,13] circ-ZNF609 has been reported to promote breast cancer cell growth, migration, and invasion, indicating the potential therapeutic effects of circ-ZNF609 in cancer therapy.[14] However, the function of circ-ZNF609 in anthracyclines-related cardiovascular disease remains largely unknown.

Herein, we investigate the role of circ-ZNF609 in DOX-induced cardiotoxicity and its underlying mechanism in vivo and in vitro. Our results show that the expression of circ-ZNF609 is regulated by RNA N^6-methyladenosine (RNA m^{6}A) methylation, whereas RNA m^{6}A demethylase fat mass and obesity associated gene (FTO) acts as the downstream factor of circ-ZNF609 in response to DOX treatment. Knockdown of circ-ZNF609 can protect the heart from DOX-induced cardiotoxicity via attenuating cardiomyocytes apoptosis, reducing intracellular and mitochondria ROS production, and ameliorating the mitochondrial nonheme iron overload, suggesting

From the [a]Cardiac Regeneration and Ageing Lab, Institute of Geriatrics (Shanghai University), Affiliated Nantong Hospital of Shanghai University (The Sixth People's Hospital of Nantong), School of Medicine, Shanghai University, Nantong, China; [b]Department of Cardiology, Shanghai Pudong New Area Gongli Hospital, Shanghai, China; [c]Department of Cardiology, Shanghai Tongji Hospital, Tongji University School of Medicine, Shanghai, China; [d]Institute of Cardiovascular Sciences, Shanghai Engineering Research Center of Organ Repair, School of Life Science, Shanghai University, Shanghai, China; and the [e]Cardiovascular Division of the Massachusetts General Hospital and Harvard Medical School, Boston, Massachusetts, USA. *Dr Yu, Mr Wang, Mr Xu, and Mr Zhao contributed equally to this work.

The authors attest they are in compliance with human studies committees and animal welfare regulations of the authors' institutions and Food and Drug Administration guidelines, including patient consent where appropriate. For more information, visit the Author Center.

Manuscript received September 23, 2022; revised manuscript received December 6, 2022, accepted December 6, 2022.

that circ-ZNF609 might be a potential therapeutic target to DOX-induced cardiotoxicity.

METHODS

ANIMAL. Adult male C57BL/6J mice (8-9 weeks of age) were purchased from Charles River Laboratories. All animal experiments were in accordance with the guidelines on the use and care of laboratory animals for biomedical research published by the National Institutes of Health (No. 85-23, revised 1996), and approved by the committee on the Ethics of Animal Experiments of Shanghai University.

To establish DOX-induced cardiotoxicity mice model, adult male C57BL/6J mice (8-9 weeks of age) were intraperitoneally injected with DOX (5 mg/kg) once a week and for 5 weeks. To study the role of circ-ZNF609, methyltransferase like 14 (METTL14) and FTO in DOX-induced cardiotoxicity, adeno associated virus 9 (AAV9) with viral titer of 10^{13} carrying circ-ZNF609 small hairpin RNA (shRNA), cardiac troponin T (cTnT) promoter-driven METTL14 shRNA, FTO shRNA, and their control in a volume of 30 μL were tail-vein injected 1 week before being subjected to DOX injection. To study the therapeutic effect of circ-ZNF609 on DOX-induced cardiotoxicity, AAV9 with viral titer of 10^{13} carrying circ-ZNF609 shRNA and their control in a volume of 30 μL were tail-vein injected at the same day after being subjected to DOX injection. Each mouse was randomly assigned to each group.

ECHOCARDIOGRAPHY. Mice were anesthetized with 3% isoflurane, and echocardiographic data were obtained through 2-dimensional targeted M-mode images, obtained in the short-axis view at the papillary muscle level using the Vevo 2100 image system (VisualSonics Inc) with a center frequency of 30 MHz. The echocardiographer was blinded to the treatment of mice. All the echocardiography parameters were presented in Supplemental Tables 1 to 6.

NEONATAL RAT CARDIOMYOCYTE ISOLATION, CULTURE, AND TREATMENT. The primary neonatal rat cardiomyocyte (NRCM) was harvested and prepared for experimental use as described previously.[15] Briefly, the left ventricles of 1- to 3-day-old neonatal rat were harvested and dissected in buffer containing 117 mM NaCl, 20 mM HEPES, 1.15 mM NaH_2PO_4, 3 mM Glucose, 5.4 mM KCl and 0.83 mM $MgSO_4$.$7H_2O$, adjusted to pH 7.4. Then, dissected tissues were digested 5 to 6 times with an enzymatic mixture compound of pancreatin (Sigma-Aldrich, P3292) and collagenase type II (Thermo Fisher Scientific, 17101-015). Then, the compound cell suspension was passed through a sterile filter screen with a 100-μm pore size (BD Falcon,352360) followed by final addition of Horse Serum (BI, 04-004-1A) to halt enzymatic digestion. The cardiomyocytes were isolated by Percoll gradient (Sigma-Aldrich, E0414) centrifugation and cultured in Dulbecco's Modified Eagle Medium (DMEM) (Sigma-Aldrich, D5796) containing 10% Horse Serum, 5% fetal bovine serum (BI, 04-001-1ACS), and 1% penicillin (Keygen, KGY0023) at 37°C in humidified air with 5% CO_2. To induce cardiotoxic injury in vitro, NRCMs were added with 0.3 μM DOX for 24 hours before harvested.

For transfecting plasmids into NRCMs, plasmids (1 μg/mL) were carried out using Lipofectamine 2000 reagent (Invitrogen) or Sino transfection reagent (Sino Biological Inc) according to the manufacturer's protocols. The efficiency of transfection was evaluated by quantitative polymerase chain reaction or western blot.

ISOLATION OF ADULT MOUSE CARDIOMYOCYTES AND CARDIAC FIBROBLAST. Adult mouse hearts were digested by retrograde perfusion on Langendorff apparatus with perfusion buffer and enzymatic solution containing 350 U/mL collagenase II (Gibco,17101-015). Briefly, adult mice were anesthetized by chloral hydrate and heparinized. Then, the chest of each of the mice was opened to expose the heart. The descending aorta was cut, and the heart was retrogradely perfused at a flow of 4 mL/min for approximately 5 minutes with perfusion buffer at 37°C containing 4 mM KCl, 135 mM NaCl, 1 mM $MgCl_2$, 0.33 mM NaH_2PO_4, 10 mM HEPES, 10 mM BDM, 10 mM glucose, and 5 mM Taurine, adjusted to pH 7.2 with NaOH. Heart tissues were gently cut into small pieces and enzymatic activity was inhibited in stop buffer containing 0.5 mg/mL bovine serum albumin and passed through a 100-μm filter to remove undigested tissues. Cardiomyocytes were sedimented at room temperature for 10 minutes at 300 rpm and then collected for further experiments.

For cardiac fibroblast, the supernatant was collected and centrifuged at 1,500 rpm for 5 minutes to obtain fibroblast and endothelial cell precipitates. The cells were then placed into a 3.5-cm petri dish/heart in the incubator (37°C, 5% CO_2, and 95% O_2) for 3 to 6 hours. After the cardiac fibroblasts adhered to the culture plate, cells were then collected for further experiments.

TUNEL STAINING. Terminal deoxynucleotidyl transferase-mediated deoxyuridine triphosphate nick end labeling (TUNEL) staining in cardiac frozen sections and NRCMs was performed using a commercial kit (Promega, #G3250). Briefly, cardiac sections or NRCMs were fixed with 4% paraformaldehyde for 15 minutes and permeabilized in 0.5% triton X-100.

After blocked, the sections or NRCMs were stained with anti-α-actinin (Sigma-Aldrich, #A7811) overnight, followed by the incubation with secondary antibodies. Then, the sections or NRCMs were equilibrized and then incubated with TUNEL reaction mixture at 37°C for 1 hour. Finally, the cell nuclei were stained by Hoechst. The fluorescence of cardiac sections was imaged by confocal microscope (LSM 710, Zeiss and LSM 880, Zeiss) while that of NRCMs were imaged by Leica microscope (DMI8). Cardiomyocytes apoptosis was calculated as the ratio of TUNEL-positive cardiomyocytes nuclei to cardiomyocytes nuclei.

MASSON STAINING. Cardiac paraffin sections were dewaxed and hydrated. Then, the sections were subjected to Masson's trichrome staining (Servicebio, #G1006) according to the manufacturer's instructions. Images were taken by Leica microscope (DM3000 LED). Image J was used to quantify the fibrotic area and the percentage of fibrosis was calculated as fibrosis areas/total myocardial areas.

SIRIUS RED STAINING. The Sirius red staining was performed to determine cardiac collagen deposition according to the manufacturer's instructions (Sbjbio, BP-DL030). Briefly, cardiac paraffin sections were dewaxed and hydrated, and were then cut into 5-μm serial sections using microtome. Slices were subjected to Sirius red staining according to the manufacturer's instruction. Images were taken by Leica microscope and Nikon microscope (ECLIPSE Ti2). Image J was used to quantify the collagen deposition area (red) and the percentage of fibrosis was calculated as collagen deposition areas/total myocardial areas.

QUANTITATIVE REAL-TIME PCR. Total RNA was isolated by RNAiso Plus (Takara, #9108). RNA concentration was measured by Nanodrop 2000 (Thermo Fisher). The RNA was converted to cDNA by using TransScript-gDNA Removal and cDNA Synthesis SuperMix (Transgen, #AT311) for the subsequent analysis of circ-ZNF609 and by using SuperScript IV Reverse (Thermo Scientific, #18090200) for the subsequent analysis of other genes according to the manufacturer's instructions. RNA levels were quantified using iTaq universal SYBR Green (Bio-rad, #1725125) by Real-Time PCR Detection System (Roche LightCycler480). Eighteen seconds was used as an internal control. For AAV9 infection rates calculation, adult cardiomyocytes were isolated from mouse hearts, DNA isolated from cardiomyocytes ($\sim 6 \times 10^6$/mouse), and the number of cardiomyocytes per mouse was accurately calculated. Serial dilutions of the scramble vector containing U6-promoter were used as a reference to obtain a standard curve for calculation. AAV9 DNA levels were quantified by real-time PCR (qPCR), and the copy number corresponding to each cycle threshold value was calculated using the tool website NEBiocalculator. Primers used in this study were listed in Supplemental Table 7.

RNA STABILITY ASSAY. For RNA stability assay, AC16 cardiomyocytes were seeded in 6-well plates. After 8-hours of transfection, the cells were treated with Actinomycin D (Selleck, S8964) and collected at different time points. Total RNA was then isolated, and the degradation rate of mRNA was analyzed by qRT-PCR and determined as previously reported.[16,17] Primers used in this study are listed in Supplemental Table 7. The degradation rate of RNA(τ) was estimated by plotting N_t/N_o against time and fitting to the following equation:

$$\frac{N_t}{N_0} = e^{-t/\tau}$$

The RNA half-life time ($t_{\frac{1}{2}}$) can be calculated from the degradation rate as follows:

$$t_{\frac{1}{2}} = \tau \bullet ln\, 2$$

t, the transcription inhibition time; τ, the degradation rate; N_t/N_o, the RNA quantities at time *t* or time *0*.

MITOCHONDRIA DNA COPY NUMBER QUANTIFICATION. For quantification of mitochondrial DNA (mtDNA) copy number, the ratio of mtDNA and genomic DNA was calculated as previously reported.[18] Briefly, mtDNA and genomic DNA were isolated from NRCM or heart tissues by using a DNA Extraction Kit (TIANGEN, DP304) according to the manufacturer's protocols. Then detection of mtDNA and genomic DNA was performed using an qPCR system. Primer sequences used in this study are listed in Supplemental Table 7.

WESTERN BLOT. The NRCMs or heart tissues were lysed using RIPA lysis buffer (KenGEN). The proteins were quantified using a BCA protein assay kit (Takara #T9300A) and then loaded onto sodium dodecyl sulphate polyacrylamide gel electrophoresis for separation. The separated proteins were electro-transferred onto polyvinylidene fluoride membranes. Then, the membranes were blocked and incubated with the appropriate primary antibodies overnight followed by incubation with horseradish peroxidase-conjugated secondary antibodies. All proteins were visualized by hypersensitive chemiluminescence kit using ChemiDoc Imaging System (Tanon, 5200S or Bio-Rad,

FIGURE 1 **circ-ZNF609 Suppression Blunts DOX-Induced Cardiotoxicity and Left Ventricular Dysfunction in Mice**

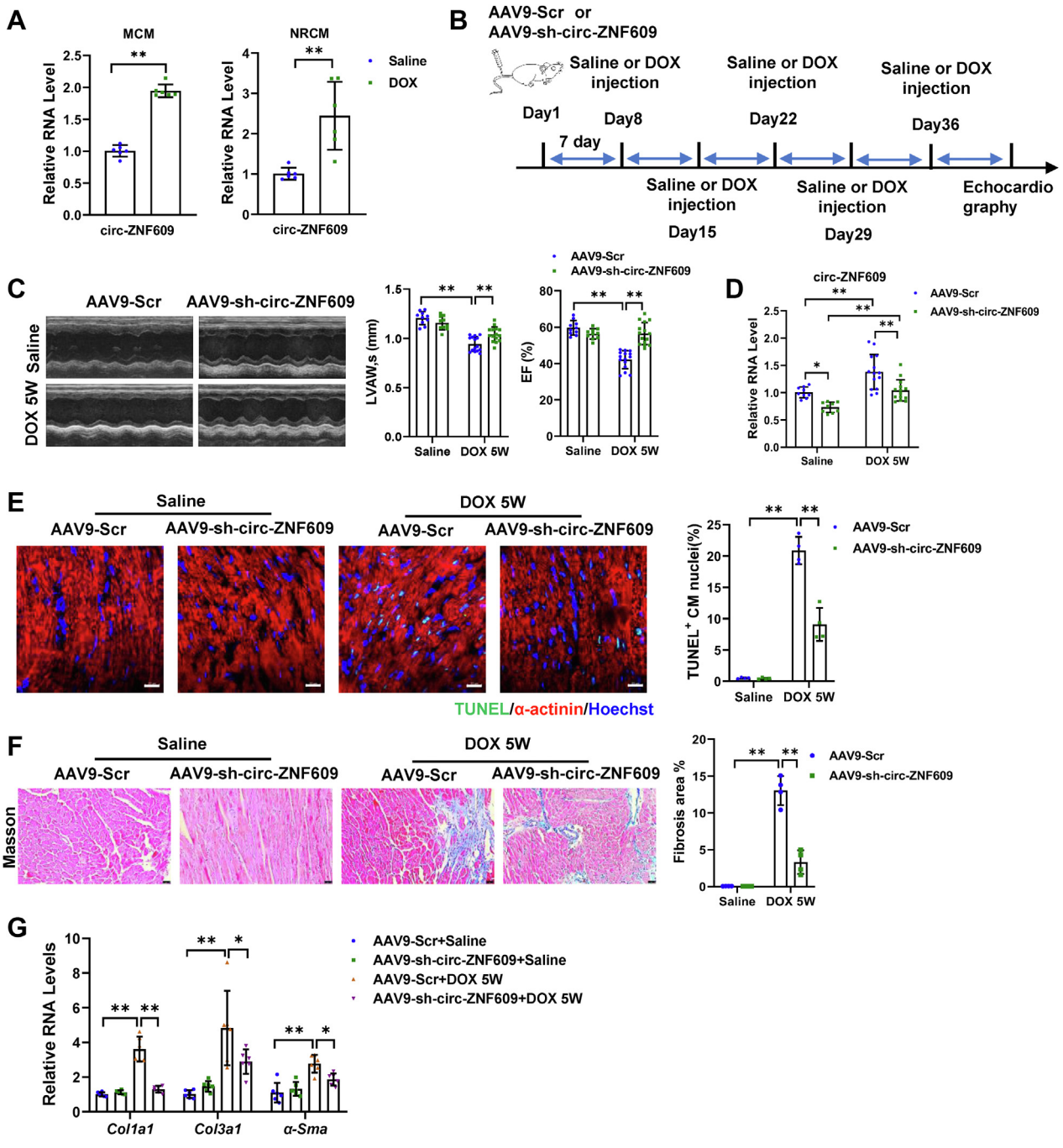

(A) The expression of circ-ZNF609 determined by quantitative real-time polymerase chain reaction (qRT-PCR) in isolated adult mouse cardiomyocytes from the doxorubicin (DOX)–treated mice hearts (**$P < 0.01$, n = 6 mice/group) and neonatal rat cardiomyocyte (NRCM) (**$P < 0.01$, n = 6 wells/group). **(B)** The schedule of adeno associated virus 9 (AAV9)-small hairpin (sh)–circ-ZNF609 virus injection and DOX-induced mice cardiotoxicity model establishment. **(C)** Preserved left ventricular ejection fraction (EF) and left ventricular anterior wall thickness (LVAWs) in the DOX-induced cardiotoxicity mice hearts treated with AAV9-sh-circ-ZNF609, as evidenced by echocardiography (**$P < 0.01$, n = 10:10:15:15 mice, respectively). **(D)** Knockdown effects of AAV9-sh-circ-ZNF609 in the mice hearts, as evidenced by qRT-PCR (*$P < 0.05$, **$P < 0.01$, n = 9:9:14:14 mice, respectively). **(E)** Attenuated myocardial apoptosis in the DOX-induced cardiotoxicity mice hearts treated with AAV9-sh-circ-ZNF609, as evidenced by terminal deoxynucleotidyl transferase deoxyuridine triphosphate nick end labelling (TUNEL) staining (**$P < 0.01$, n = 4 mice/group, scale bar = 20 μm). **(F)** Reduced cardiac fibrosis in the DOX-induced cardiotoxicity mice hearts treated with AAV9-sh-circ-ZNF609, as evidenced by Masson's staining (**$P < 0.01$, n = 4 mice/group, scale bar = 25 μm). **(G)** Decreased expression of the fibrotic-associated genes (*α-Sma*, *Col1a1*, and *Col3a1*) in the DOX-induced cardiotoxicity mice hearts treated with AAV9-sh-circ-ZNF609 (*$P < 0.05$, **$P < 0.01$, n = 6 mice/group). Data are presented as mean ± SD. (**A**, Student *t* test. **C to G**, 2-way analysis of variance with Tukey post hoc test.) CM = cardiomyocyte; MCM = adult mouse cardiomyocyte; Scr = scramble.

FIGURE 2 Knockdown of circ-ZNF609 Ameliorates DOX-Induced Cardiotoxicity Via Preventing Cardiomyocytes Apoptosis and Oxidative Stress

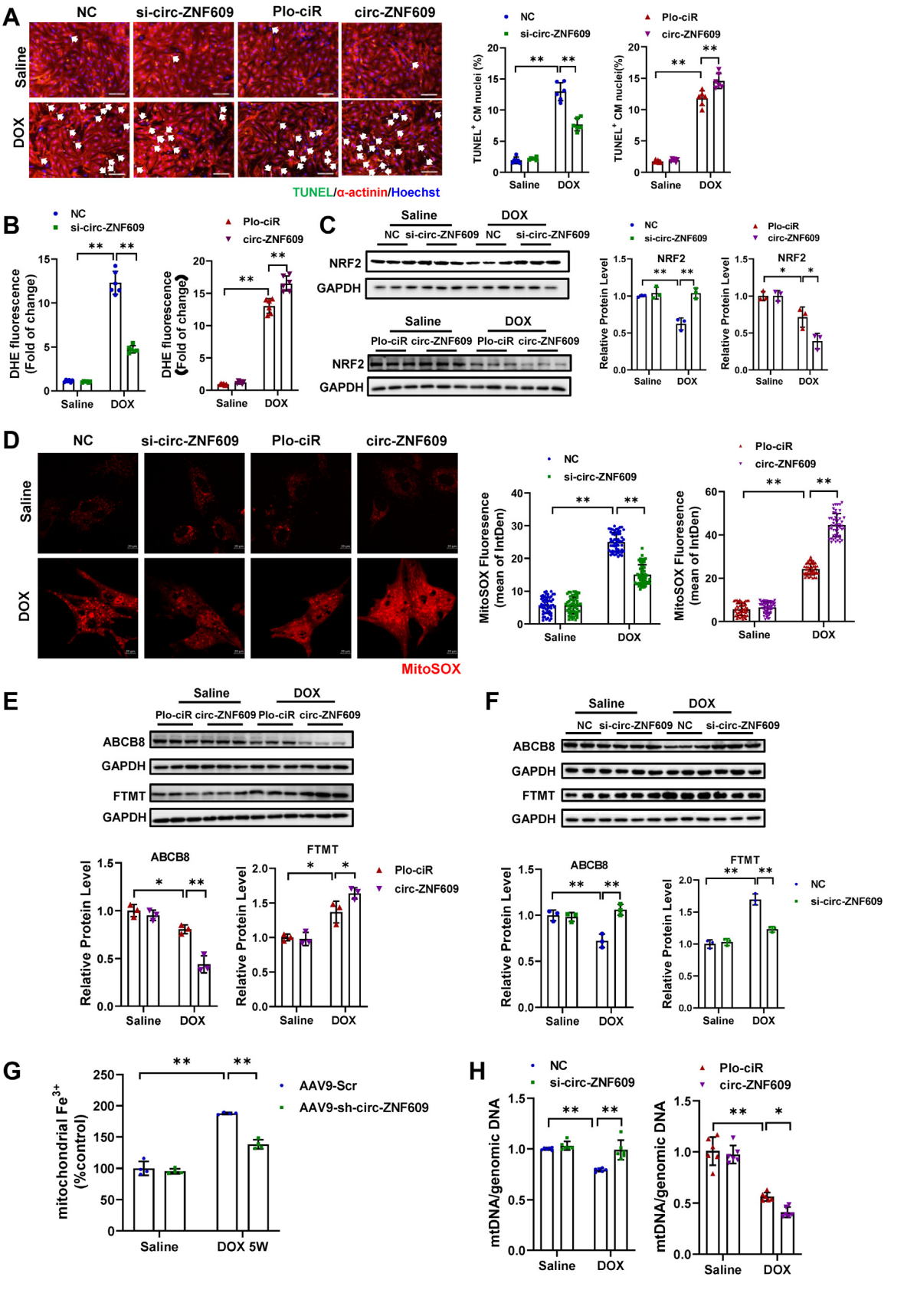

Continued on the next page

17001402). Band intensity was calculated using Image J. Antibodies used in this study were listed in Supplemental Table 8.

RNA m^{6}A METHYLATION QUANTIFICATION. Total RNAs were extracted from murine hearts by miRNeasy Mini Kit (QIAGEN, #217004) with DNase I on column treatment. Then, the RNA m^{6}A methylation quantification kit (Colorimetric) (Abcam, #ab185912) was used according to the manufacturer's protocols. Briefly, 200 ng of total RNA were added after RNA binding, m^{6}A RNA capture, and signal detection. Relative quantification of RNA m^{6}A was calculated as recommended by the manufacturer.

DOT BLOT. The total RNA was isolated by miRNeasy Mini Kit (QIAGEN, #217004) with DNase I on column treatment. RNA was pre-denatured for 10 minutes at 70°C, then RNA was loaded onto the Hybond-N$^+$ membrane. The membrane was further crosslinked by ultraviolet light. The samples were incubated with m^{6}A antibodies (Abclonal, #A19841) at 4°C overnight. The membranes were incubated with rabbit immunoglobulin G antibody coupled to horseradish peroxidase. Finally, the dots were visualized by hypersensitive chemiluminescence kit using ChemiDoc Imaging System (Bio-Rad, 17001402). Methylene blue staining was used to confirm the equal amounts of RNA samples.

DETECTION OF MITOCHONDRIAL FE^{3+}. The mitochondrial Fe^{3+} (nonheme iron) was measured by spectrophotometry using the iron assay kit (Abcam, #ab83366) according to the manufacturer's protocol. Briefly, mitochondria were first isolated from tissues samples with a Mitochondria Isolation Kit (Beyotime, C3606) according to the manufacturer's protocols. Then, mitochondria samples and standards were added to a 96-wells enzyme-linked immunosorbent assay plate. Samples were incubated with iron reducer at 37°C for 30 minutes for measuring total iron ion concentration or without for measuring Fe^{2+} concentration. Then, the iron probe was added to each well and incubated for 60 minutes at 37°C. The plate was analyzed with a microplate reader. The mitochondrial Fe^{3+} concentration is equal to mitochondrial total iron ion concentration minus mitochondrial Fe^{2+} concentration, and it was displayed as its proportion of total iron ion.

DETECTION OF ROS. ROS production was determined by using DHE staining kit (US Everbright, D1008) and MitoSOX Red kit (Yeasen, 40778ES50). Both kits were used according to the manufacturer's protocols. Briefly, NRCMs were incubated in DMEM containing 10 μM dihydroethidium (DHE) for 90 minutes or Hank's solution containing 5 μM mitoSOX Red for 30 minutes before being harvested at 37°C in the dark. After being washed with phosphate-buffered saline or Hank's, DHE staining of NRCMs was imaged by Leica microscope (DMI8, Germany) and MitoSOX staining of NRCMs was captured by confocal microscope (LSM880, Zeiss). The fluorescence intensity of NRCMs was analyzed using Image J.

STATISTICAL ANALYSIS. Data were presented as the mean ± SD. Normal distributions of all data were tested by using Shapiro-Wilk or Kolmogorov-Smirnov tests. For data following normal distributions, comparisons between 2 groups were performed using the Student *t* test, whereas comparisons among >2 groups used 2-way analysis of variance followed by Tukey's post hoc test for multiple pairwise comparisons. For data that did not follow normal distributions, a Mann-Whitney *U* test (2 groups) or Kruskal-Wallis test (>2 groups) was used. Analyses were performed using GraphPad Prism 8.0 and SPSS 20.0 software (SPSS Inc). A $P < 0.05$ was considered statistically significant.

FIGURE 2 Continued

(A) Representative images of immunofluorescence staining and quantification of the TUNEL positive cardiomyocytes in the DOX-treated NRCM transfected with or without small interfering (si)-circ-ZNF609 or circ-ZNF609 (**$P < 0.01$, n = 6 wells/group, scale bar = 100 μm). **(B)** Intracellular reactive oxygen species (ROS) level in the DOX-treated NRCM transfected with or without si-circ-ZNF609 or circ-ZNF609, as evidenced by dihydroethidium (DHE) staining (**$P < 0.01$, n = 6 wells/group). **(C)** Western blot analysis of NRF2 in the DOX-treated NRCM transfected with or without si-circ-ZNF609 or circ-ZNF609 (*$P < 0.05$, **$P < 0.01$, n = 3 wells/group). **(D)** Representative images of immunofluorescence staining and quantification of mitochondrial ROS level in the DOX-treated NRCM transfected with or without si-circ-ZNF609 or circ-ZNF609, as evidenced by MitoSOX red staining (**$P < 0.01$, n = 50 cardiomyocytes/group, scale bar = 20 μm). **(E, F)** Western blot analysis of ABCB8 and FTMT in the DOX-treated NRCM transfected with or without circ-ZNF609 (*$P < 0.05$, **$P < 0.01$, n = 3 wells/group) or si-circ-ZNF609 (**$P < 0.01$, n = 3 wells/group). **(G)** Mitochondrial nonheme iron (Fe^{3+}) in the DOX-induced cardiotoxicity mice hearts injected with or without AAV9-sh-circ-ZNF609 (**$P < 0.01$, n = 4 mice/group). **(H)** The mitochondrial DNA levels in the DOX-treated NRCM transfected with or without si-circ-ZNF609 or circ-ZNF609 (*$P < 0.05$, **$P < 0.01$, n = 6 wells/group). Data are presented as mean ± SD. (**A to C**, 2-way analysis of variance (ANOVA) with Tukey's post hoc test. **D**, **Left**: 2-way ANOVA by Tukey test; **right**: Kruskal-Wallis test. **E to H**, 2-way ANOVA with Tukey's post hoc test.) NC = negative control; NRF2 = nuclear factor erythroid 2- related factor 2; Plo-ciR = empty vector without circ-ZNF609 overexpression; other abbreviations as in Figure 1.

FIGURE 3 Circ-ZNF609 Negatively Regulates the Expression of RNA m^{6}A Demethylase FTO and Contributes to DOX-Induced Cardiotoxicity Regulation

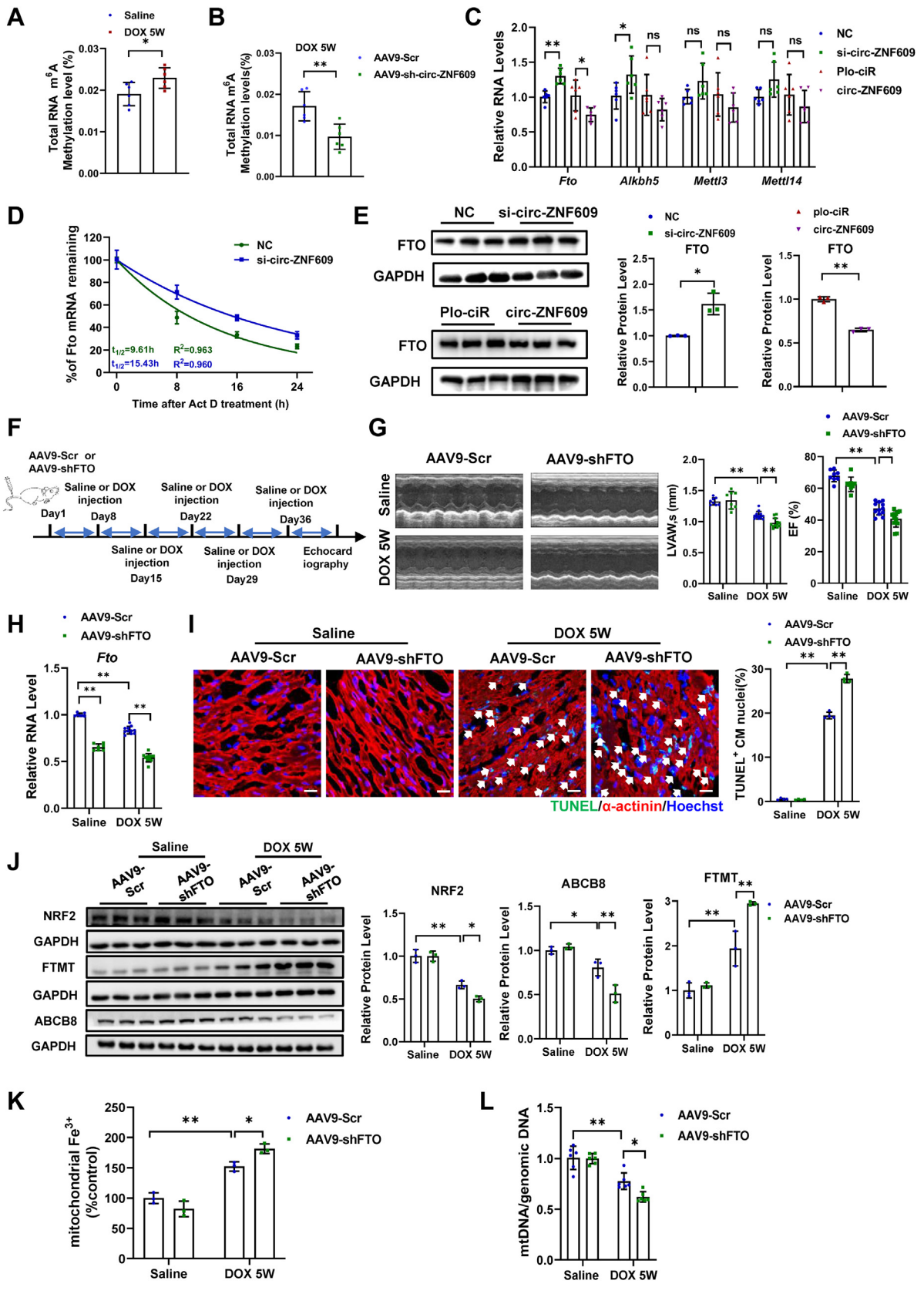

Continued on the next page

RESULTS

CIRC-ZNF609 SUPPRESSION BLUNTS DOX-INDUCED CARDIOTOXICITY AND LEFT VENTRICULAR DYSFUNCTION IN MICE. To explore the potential role of circ-ZNF609 in regulating DOX-induced cardiotoxicity, we first quantified the expression of circ-ZNF609 in isolated adult mouse cardiomyocytes from the DOX-treated mice hearts and DOX-treated cultured NRCMs by qRT-PCR. As shown in **Figure 1A**, after intraperitoneal injection with DOX for 5 weeks, the expression of circ-ZNF609 was significantly increased in the adult mouse cardiomyocytes of DOX-treated mice and in the NRCMs treated with DOX. Thus, we tested whether inhibition of circ-ZNF609 could prevent DOX-induced cardiotoxicity. We manipulated the expression of circ-ZNF609 in murine heart by tail vein injection of AAV9-sh-circ-ZNF609, which was generated as previously reported.[11] Then, DOX-induced cardiotoxicity murine model was established and used to explore the function of circ-ZNF609 inhibition (**Figure 1B**). As measured by echocardiography, we found that circ-ZNF609 knockdown preserved cardiac function and inhibited the thinning of ventricular wall thickness as indicated by preserved ejection fraction (EF), and left ventricular anterior wall thickness in systole (LVAWs) (**Figure 1C**). The knockdown effect of AAV9-sh-circ-ZNF609 was verified by qRT-PCR (**Figure 1D**). Next, we assessed the cardiac apoptosis and fibrosis in DOX-induced cardiotoxicity. As shown in **Figure 1E**, TUNEL staining showed that the administration of AAV9-sh-circ-ZNF609 significantly reduced the apoptosis induced by DOX-treatment in the hearts. Consistently, western blot showed that knockdown of circ-ZNF609 led to decreased expression of Bax/Bcl-2, indicating a protective effect of circ-ZNF609 inhibition against DOX-induced apoptosis in the hearts (Supplemental Figure 1A). In addition, Masson staining and Sirius red staining suggested that cardiac fibrosis was attenuated by the knockdown of circ-ZNF609 in the DOX group (**Figure 1F**, Supplemental Figure 1B). Meanwhile, the expression of fibrotic genes (*Col1a1*, *Col3a1*, and α-*Sma*) was decreased after AAV9-sh-circ-ZNF609 administration (**Figure 1G**). Taken together, our data reveal that circ-ZNF609 is involved in the regulation of DOX-induced cardiotoxicity and circ-ZNF609 knockdown protects against DOX-induced cardiotoxicity via improving cardiac function, reducing cardiomyocytes apoptosis, and attenuating cardiac fibrosis.

KNOCKDOWN OF CIRC-ZNF609 AMELIORATES DOX-INDUCED CARDIOTOXICITY VIA PREVENTING CARDIOMYOCYTES APOPTOSIS AND OXIDATIVE STRESS. Then, we examined the role of circ-ZNF609 in cultured NRCM in response to DOX-treatment. The circ-ZNF609 overexpression construct and small interfering RNA (siRNA) were used as previously reported.[11] Knockdown of circ-ZNF609 inhibited DOX-induced NRCM apoptosis whereas overexpression of circ-ZNF609 led to a significant exacerbation of apoptosis as determined by TUNEL staining and western blot of Bax/Bcl-2 ratio (**Figure 2A,** Supplemental Figures 2A and 2B). In addition, DHE staining suggested that circ-ZNF609 suppression reduced the formation of ROS induced by DOX in NRCM whereas circ-ZNF609 overexpression increased it (**Figure 2B**). Transcription factor NRF2 is considered as a classic regulator in DOX-induced cardiotoxicity due to the fact that it can activate antioxidant genes and plays key roles in response to oxidative stress.[19] Therefore, we detected the expression of NRF2 and found that it can be negatively regulated by circ-ZNF609 under DOX-treatment (**Figure 2C**). Oxidative stress derived from mitochondria is a causative mechanism underlying

FIGURE 3 Continued

(A) The increased total RNA N^6 methyladenosine (RNA m^6A) level in the mice heart from DOX-induced cardiotoxicity model (*$P < 0.05$, n = 6 mice/group). **(B)** The decreased total RNA m^6A level in the mice hearts from DOX-induced cardiotoxicity treated with AAV9-sh-circ-ZNF609 (**$P < 0.01$, n = 6 mice/group). **(C)** qRT-PCR analysis showed the expression levels of m^6A writers (*Mettl14* and *Mettl3*) and eraser (*Fto* and *Alkbh5*) in the NRCM treated with or without circ-ZNF609 overexpression or knockdown (*$P < 0.05$, **$P < 0.01$, n = 6 wells/group). **(D)** Degradation curves showed the level of fat mass and obesity associated gene (*Fto*) mRNA in NRCM transfected with or without si-circ-ZNF609 after treated with actinomycin D for 0, 8, 16, and 24 hours, as evidenced by qRT-PCR (**$P < 0.01$, n = 6 wells/group). **(E)** Western blot analysis revealed the expression level of FTO in the NRCM treated with or without circ-ZNF609 overexpression or knockdown (*$P < 0.05$, **$P < 0.01$, n = 3 wells/group). **(F)** The schedule of AAV9-shFTO virus injection and DOX-induced mice cardiotoxicity model establishment. **(G)** Representative echocardiographic images of EF and LVAWs of DOX-induced cardiotoxicity mice model injected with or without AAV9-shFTO (**$P < 0.01$, n = 8:8:12:12 mice, respectively). **(H)** Knockdown effects of AAV9-shFTO in the mice heart, as evidenced by qRT-PCR (**$P < 0.01$, n = 7:7:11:11 mice, respectively). **(I)** Representative images of immunofluorescence staining and quantification of the TUNEL-positive cardiomyocytes in the DOX-induced cardiotoxicity mice hearts injected with or without AAV9-shFTO (**$P < 0.01$, n = 4 mice/group, scale bar = 20 μm). **(J)** Western blot analysis of NRF2, ABCB8, and FTMT in the DOX-induced cardiotoxicity mice hearts injected with or without AAV9-shFTO (*$P < 0.05$, **$P < 0.01$, n = 3 mice/group). **(K)** Mitochondrial nonheme iron (Fe^{3+}) in the DOX-induced cardiotoxicity mice hearts injected with or without AAV9-shFTO (*$P < 0.05$, **$P < 0.01$, n = 3 mice/group). **(L)** The mitochondrial DNA level in the DOX-induced cardiotoxicity mice hearts injected with or without AAV9-shFTO (*$P < 0.05$, **$P < 0.01$, n = 6 mice/group). All data are expressed as mean ± SD. (**A to E**, Student *t* test. **G to L**, 2-way ANOVA with Tukey's post hoc test.) Abbreviations as in **Figures 1 and 2**.

FIGURE 4 FTO Overexpression Abrogates the Deteriorating Effect of circ-ZNF609 on DOX-Induced Cardiomyocyte Apoptosis and Oxidative Stress

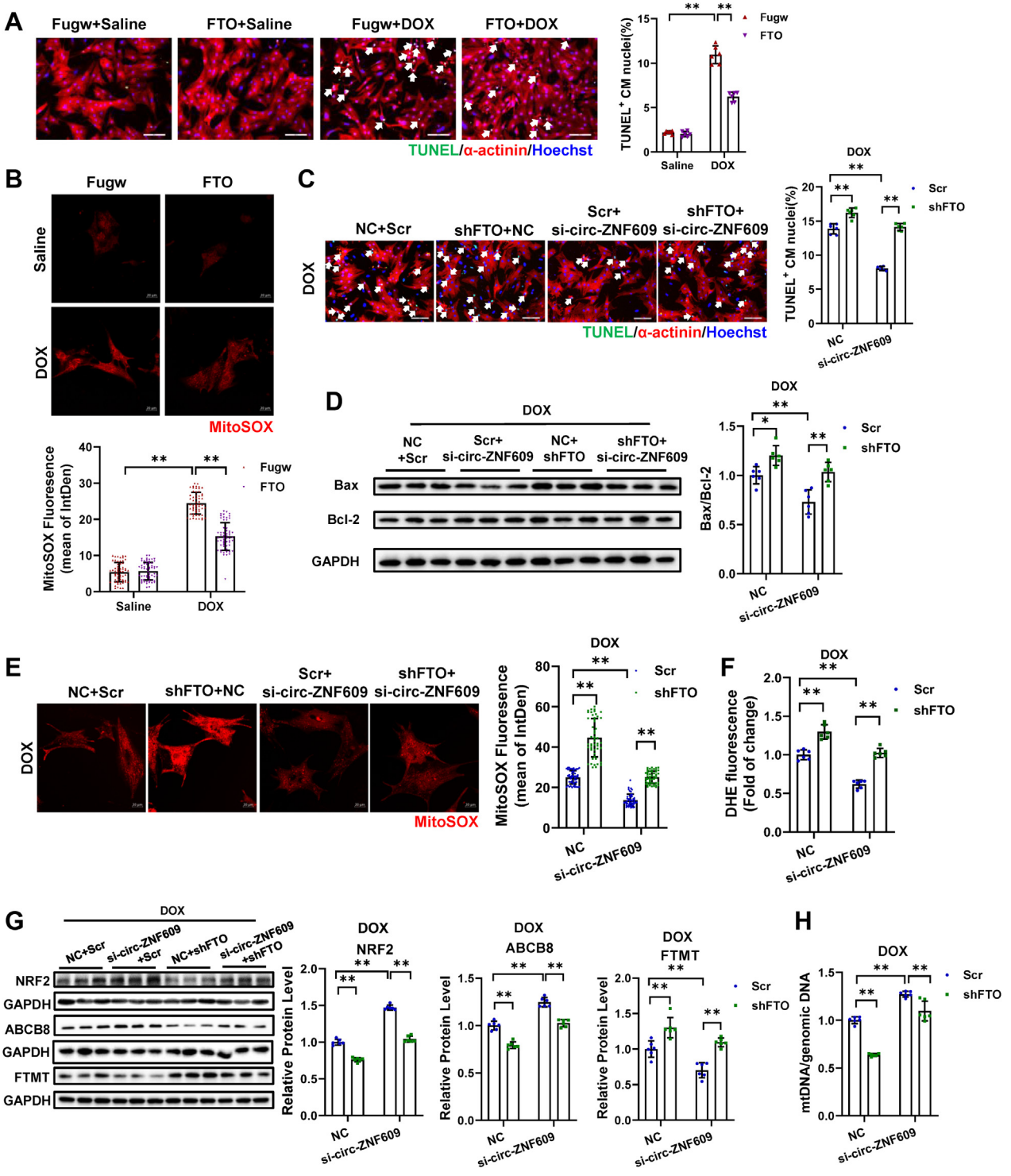

Continued on the next page

DOX-induced cardiotoxicity; however, a recent study has shown that iron could cause formation of ROS and lipid peroxidation under conditions of DOX.[20] Therefore, we detected the ROS content in mitochondria, as evidenced by MitoSOX staining (Thermo Fisher Scientific), and found that knockdown of circ-ZNF609 attenuated mitochondria ROS accumulation in the DOX-induced cardiotoxicity in vitro (**Figure 2D**). It has been previously reported that mitochondrial iron storage protein ferritin (FTMT) and mitochondrial transporter ABCB8 are protein markers of mitochondrial iron metabolic dysfunction, which leads to mitochondrial ROS generation and is associated with myocytes ferroptosis, a type of regulated cell death caused by the redox state disorder of intracellular microenvironment.[21,22] As shown by western blot, the protein level of FTMT was upregulated and ABCB8 were also downregulated in DOX-treated NRCMs. circ-ZNF609 overexpression exerted further additional upregulation of FTMT and reduction of ABCB8 whereas knockdown of circ-ZNF609 reversed the effects of DOX on FTMT and ABCB8 (**Figures 2E and 2F**). Similarly, the regulatory effects of circ-ZNF609 inhibition on FTMT, ABCB8, and NRF2 were also observed in the DOX-treated mice hearts (Supplemental Figure 3A). Then, we isolated mitochondria from the cardiomyocytes, and found that DOX treatment significantly increased the Fe^{3+} (nonheme iron) in the mitochondria, whereas circ-ZNF609 knockdown alleviated the accumulation of Fe^{3+} in the heart tissues of DOX-treated mice (**Figure 2G**). Moreover, reduction of the mitochondrial DNA copy number which was induced by DOX-treatment in the hearts and NRCM was also alleviated by circ-ZNF609 knockdown, whereas circ-ZNF609 overexpression in NRCM aggravated it (**Figure 2H**, Supplemental Figure 3B). Collectively, these results suggest that circ-ZNF609 knockdown ameliorates DOX-induced cardiotoxicity through attenuating cardiomyocytes apoptosis, reducing ROS accumulation, and alleviating cardiotoxicity caused by mitochondrial iron overload after DOX treatment.

CIRC-ZNF609 NEGATIVELY REGULATES THE EXPRESSION OF RNA m^{6}A DEMETHYLASE FTO AND CONTRIBUTES TO DOX-INDUCED CARDIOTOXICITY REGULATION. circ-ZNF609 has been reported to have m^{6}A modification and RNA m^{6}A methylation contributed to the regulatory effects of circ-ZNF609 on cardiac ischemia/reperfusion injury in our previous study.[11] We found that total RNA m^{6}A methylation was elevated in DOX-induced cardiotoxicity (**Figure 3A**). We then sought to discover whether RNA m^{6}A methylation was involved in the protective effects of circ-ZNF609 inhibition on DOX-induced cardiotoxicity. As shown in **Figure 3B**, circ-ZNF609 knockdown decreased the total RNA m^{6}A methylation level in DOX-induced cardiotoxicity. Next, to investigate the underlying mechanism of RNA m^{6}A alteration in response to circ-ZNF609 inhibition in DOX-induced cardiotoxicity, we screened the known effectors of m^{6}A modification by qRT-PCR and found that RNA m^{6}A demethylase FTO was negatively regulated by circ-ZNF609 (**Figure 3C**). Then, actinomycin D assay results suggested that silencing of circ-ZNF609 could inhibit the *Fto* mRNA degradation (**Figure 3D**). Furthermore, by western blot assay, we confirmed that circ-ZNF609 could negatively regulate the protein level of FTO in NRCMs and mice hearts (**Figure 3E**, Supplemental Figure 4A). Taken together, these data suggest that circ-ZNF609 negatively regulates the expression of RNA m^{6}A demethylase FTO and contributes to RNA m^{6}A methylation regulation.

RNA m^{6}A demethylase FTO has been found to be implicated in heart failure.[17,23] However, its role in

FIGURE 4 Continued

(A) Representative images of immunofluorescence staining and quantification of the TUNEL-positive cardiomyocytes displayed the protective effect of FTO overexpression on cardiomyocytes apoptosis in the DOX-treated NRCM (**$P < 0.01$, n = 6 wells/group, scale bar =100 μm). **(B)**. Representative images of immunofluorescence staining and quantification of the mitochondrial ROS level displayed the protective effect of FTO overexpression on oxidative stress in the DOX-treated NRCM (**$P < 0.01$, n = 50 cardiomyocytes/group, scale bar = 20 μm). **(C)** Representative images of immunofluorescence staining and quantification of the TUNEL-positive cardiomyocytes displayed the block effect of FTO knockdown on circ-ZNF609 inhibition in the DOX-treated NRCM (**$P < 0.01$, n = 6 wells/group, scale bar = 100 μm). **(D)** Western blot analysis of Bax and Bcl-2 revealed the block effect of FTO knockdown on circ-ZNF609 inhibition in the DOX-treated NRCM (*$P < 0.05$, **$P < 0.01$, n = 6 wells/group). **(E)** Representative images of immunofluorescence staining and quantification of the mitochondrial ROS level displayed the disrupt effect of FTO knockdown on circ-ZNF609 inhibition in the DOX-treated NRCM (**$P < 0.01$, n = 50 cardiomyocytes/group, scale bar = 20 μm). **(F)** Quantification of intracellular ROS revealed the block effect of FTO knockdown on circ-ZNF609 inhibition in the DOX-treated NRCM, as evidenced by DHE staining (**$P < 0.01$, n = 6 wells/group). **(G)** Western blot analysis of NRF2, ABCB8, and FTMT revealed the block effect of FTO knockdown on circ-ZNF609 inhibition in the DOX-treated NRCM (**$P < 0.01$, n = 6 wells/group). **(H)** The analysis of mitochondrial DNA level revealed the block effect of FTO knockdown on circ-ZNF609 suppression in the DOX-treated NRCM (**$P < 0.01$, n = 6 wells/group). All data are expressed as mean ± SD. (**A**, 2-way ANOVA with Tukey's post hoc test. **B**, Kruskal-Wallis test. **C and D**, 2-way ANOVA with Tukey's post hoc test. **E**, Kruskal-Wallis test. **F to H**, 2-way ANOVA with Tukey's post hoc test.) Fugw = empty vector without FTO overexpression; other abbreviations as in **Figures 1-3**.

FIGURE 5 RNA m^{6}A Methylation Regulates the Stability of circ-ZNF609 and Participates in DOX-Induced Cardiotoxicity

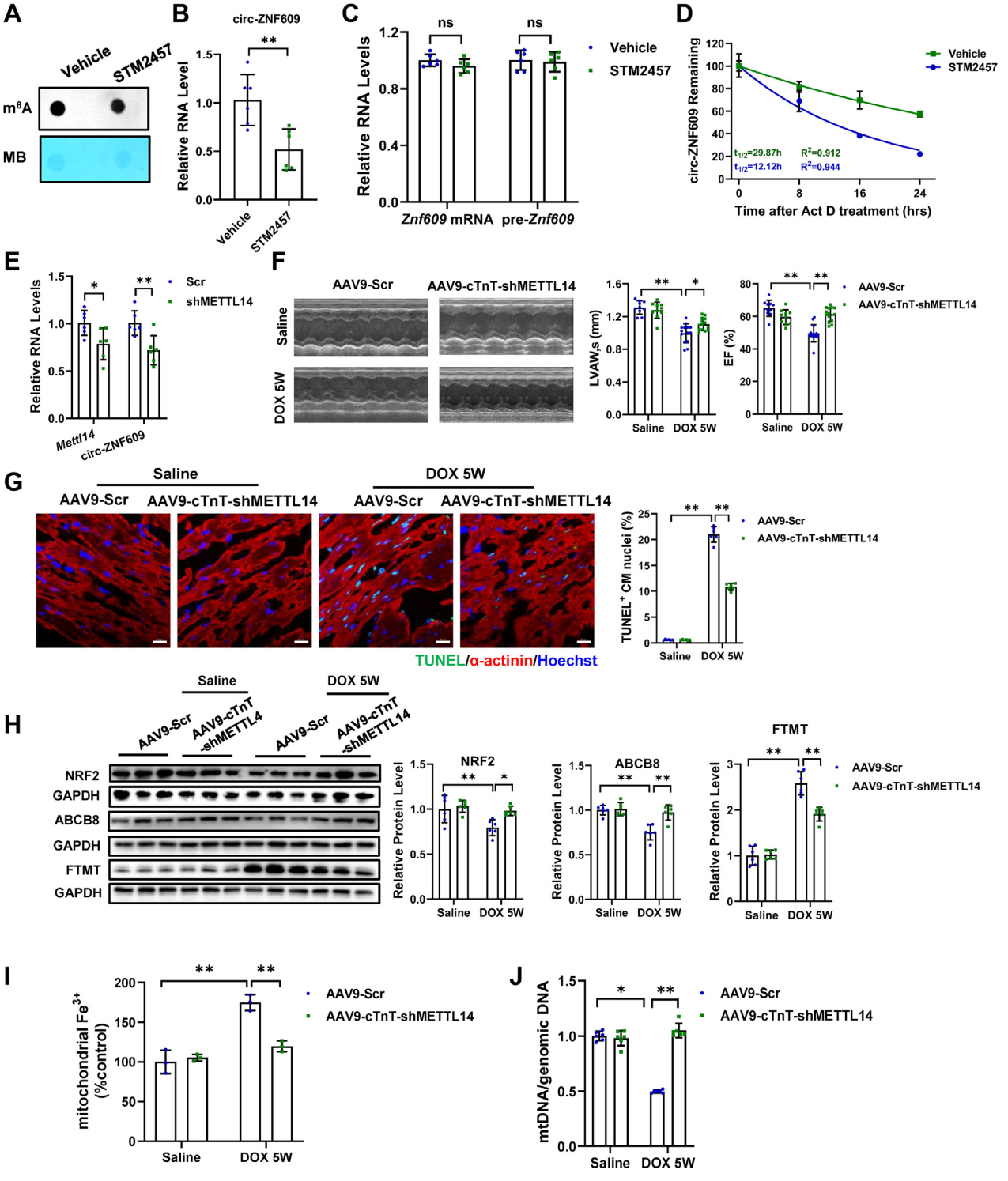

Continued on the next page

DOX-induced cardiotoxicity remains unknown. We found that FTO was downregulated by DOX-treatment in the mice hearts (Supplemental Figure 4B). To examine whether FTO was involved the regulation of DOX-induced cardiotoxicity, we generated shFTO construct and delivered AAV9-shFTO to adult mice via tail vein injection. One week after AAV9-shFTO administration, mice were subjected to intraperitoneal injection of DOX or saline for 5 weeks (**Figure 3F**). As suggested by echocardiography, FTO knockdown deteriorated cardiac function (EF) in DOX-treated mice and decreased ventricular anterior wall thickness (LVAWs) (**Figure 3G**). The knockdown effects of AAV9-shFTO were verified by qRT-PCR (**Figure 3H**). The DOX-treatment induced cardiomyocytes apoptosis was aggravated after FTO knockdown as determined by TUNEL staining and Bax/Bcl-2 ratio in western blot (**Figure 3I**, Supplemental Figure 4C). Also, Masson staining, Sirius red staining, and qRT-PCR analysis of fibrotic genes (*Col1a1*, *Col3a1*, and α-*Sma*) suggested that DOX-induced cardiac fibrosis was further increased after FTO knockdown (Supplemental Figures 4D to 4F). In addition, western blot of NRF2, FTMT, and ABCB8 revealed the exacerbated oxidative stress and iron overload (**Figure 3J**). Furthermore, this nonheme iron accumulation in mitochondria was also confirmed by Fe^{3+} measurement in the DOX-induced cardiotoxicity mice hearts treated with AAV9-shFTO (**Figure 3K**). Moreover, the mitochondrial DNA content was also significantly decreased in FTO knockdown, indicating the aggravated imbalance of mtDNA biogenesis and deposition in DOX-treated heart tissue (**Figure 3L**). These data indicate that circ-ZNF609 negatively regulates the expression of RNA m^6A demethylase FTO, and FTO might act as the downstream factor of circ-ZNF609 in regulating DOX-induced cardiotoxicity.

FTO OVEREXPRESSION ABROGATES THE DETERIORATING EFFECT OF CIRC-ZNF609 ON DOX-INDUCED CARDIOMYOCYTE APOPTOSIS AND OXIDATIVE STRESS. Next, we investigated whether FTO acted as the downstream factor of circ-ZNF609 in DOX-induced cardiomyocyte apoptosis and oxidative stress. FTO overexpression and knockdown were generated, and effects were confirmed (Supplemental Figures 5A and 5B). FTO overexpression significantly reduced DOX-treatment induced cardiomyocyte apoptosis, as well as mitochondria ROS content (**Figures 4A and 4B**). Conversely, FTO knockdown further aggravated apoptosis and mitochondrial ROS accumulation (Supplemental Figures 5C and 5D). Furthermore, we explored whether FTO was a key downstream factor of circ-ZNF609's effects in DOX-treated NRCMs. Functional rescue assays were performed by cotransfecting circ-ZNF609 siRNA, and FTO shRNA. FTO suppression could reverse the protective effect of circ-ZNF609 inhibition on DOX-treated NRCM, as evidenced by TUNEL staining, western blot of Bax/Bcl-2 ratio, mitoSOX staining, and DHE staining (**Figures 4C to 4F**). In addition, western blot detection of NRF2, FTMT, and ABCB8 also showed that effects of si-circ-ZNF609 on regulating those proteins expression were abolished by FTO knockdown (**Figure 4G**). Moreover, the mtDNA copy number which was maintained by circ-ZNF609 knockdown was disrupted by FTO inhibition in DOX treatment (**Figure 4H**). In summary, these results suggest that FTO functions as a downstream effector of circ-ZNF609 in regulating DOX-induced cardiotoxicity.

RNA m^6A METHYLATION REGULATES THE STABILITY OF CIRC-ZNF609 AND PARTICIPATES IN DOX-INDUCED CARDIOTOXICITY. RNA m^6A methylation has been detected in circ-ZNF609 and could modulate circRNA metabolism; however, whether the m^6A methylation is involved in the regulation of circ-ZNF609 in

FIGURE 5 Continued

(A) Dot blot of RNA m^6A levels in NRCM treated with RNA m^6A inhibitor STM2457. **(B)** qRT-PCR analysis showed the expression level of circ-ZNF609 in the NRCM treated with STM2457 (**$P < 0.01$, n = 6 wells/group). **(C)** The expression level of *Znf609* mRNA and pre-*Znf609* in the NRCM treated with STM2457 (n = 6 wells/group). **(D)** The stability of circ-ZNF609 in cardiomyocytes with or without STM2457 treatment after treated with actinomycin D (Act D) for 0, 8, 16, and 24 hours, as evidenced by qRT-PCR (*$P < 0.05$, **$P < 0.01$, n = 6 wells/group). **(E)** The expression of *Mettl14* and circ-ZNF609 in NRCM treated with shMETTL14 (*$P < 0.05$, **$P < 0.01$, n = 6 wells/group). **(F)** Preserved EF and LVAWs in the DOX-induced cardiotoxicity mice hearts treated with or without AAV9-cTnT-shMETTL14, as evidenced by echocardiography (*$P < 0.05$, **$P < 0.01$, n = 10:10:14:14 mice, respectively). **(G)** Representative images of immunofluorescence staining and quantification of the TUNEL-positive cardiomyocytes in the DOX-induced cardiotoxicity mice hearts treated with or without AAV9-cTnT-shMETTL14 (**$P < 0.01$, n = 6 mice/group, scale bar = 20 μm). **(H)** Western blot analysis of NRF2, ABCB8, and FTMT in the DOX-induced cardiotoxicity mice hearts treated with or without AAV9-cTnT-shMETTL14 (*$P < 0.05$, **$P < 0.01$, n = 6 mice/group). **(I)** Mitochondrial nonheme iron (Fe^{3+}) in the DOX-induced cardiotoxicity mice hearts injected with or without AAV9-cTnT-shMETTL14 (**$P < 0.01$, n = 3 mice/group). **(J)** The mitochondrial DNA level in the DOX-induced cardiotoxicity mice hearts treated with or without AAV9-cTnT-shMETTL14 (*$P < 0.05$, **$P < 0.01$, n = 6 mice/group). All data are expressed as mean ± SD. (**B to E**, Student *t* test. **F**, **Left**: 2-way ANOVA with Tukey's post hoc test, **right**: Kruskal-Wallis test. **G to J**, 2-way ANOVA with Tukey's post hoc test). cTnT = cardiac troponin T; MB = methylene blue staining; other abbreviations as in **Figures 1 and 3**.

FIGURE 6 The Protective Effects of METTL14-mediated m^{6}A Modification on DOX-Induced Cardiomyocyte Apoptosis and Oxidative Stress Are Disrupted by circ-ZNF609 Overexpression

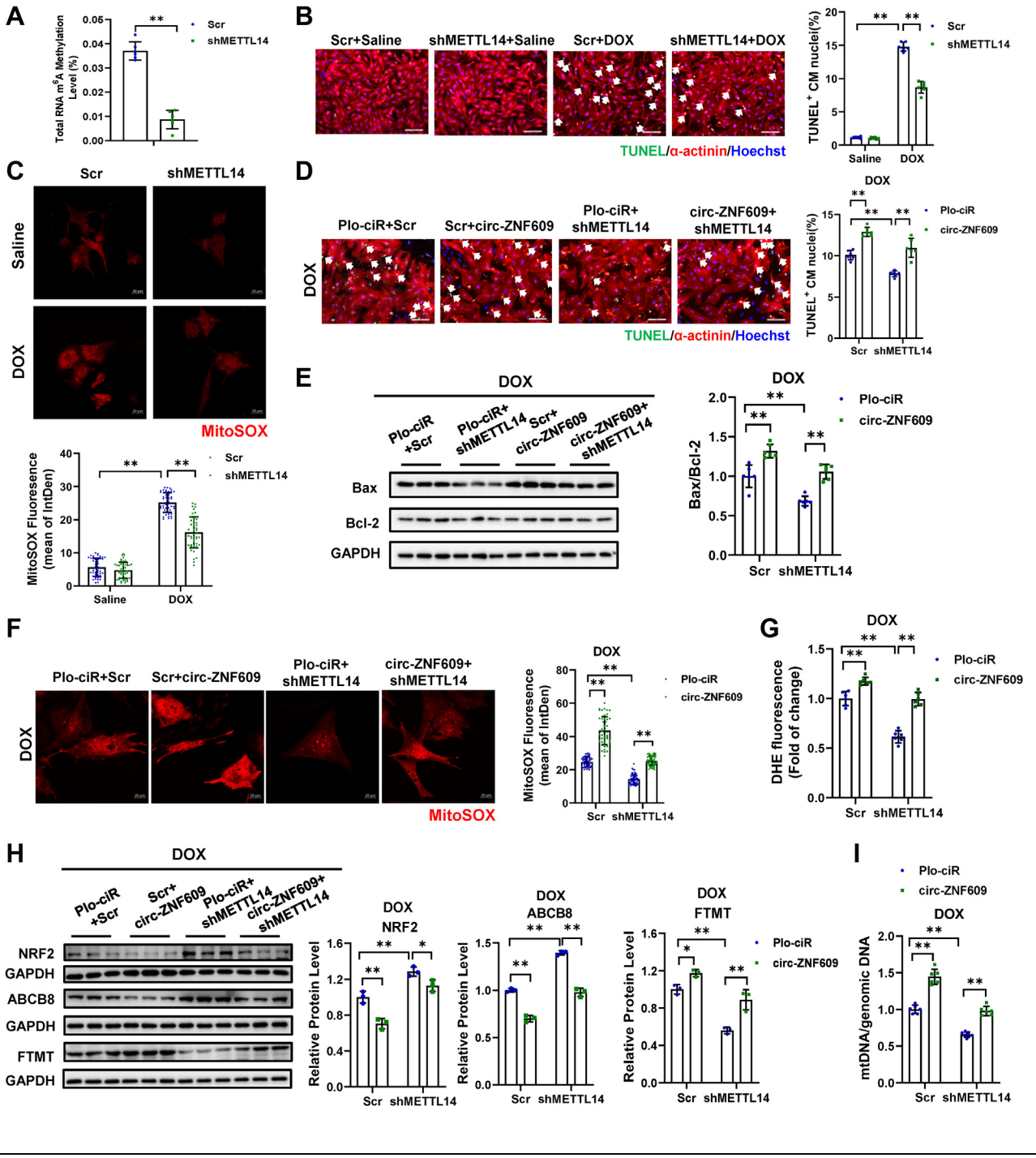

Continued on the next page

cardiomyocytes remains unknown.[24] Thus, we explored the regulatory role of m^{6}A methylation on circ-ZNF609. Small molecular inhibitor STM2457, which is a potent RNA methyltransferase inhibitor and selectively binds to the METTL3-METTL14 heterodimer, was used to reduce RNA m^{6}A levels in NRCM.[25] As shown in **Figures 5A and 5B**, total RNA m^{6}A methylation level was decreased after STM2457

treatment, and this RNA m^{6}A methylation suppression significantly decreased circ-ZNF609 expression level. Interestingly, STM2457 caused no alteration on the expression level of linear mRNA *Znf609* and precursor *Znf609* (pre-*Znf609*) in NRCM, indicating that RNA m^{6}A did not affect the biogenesis of circ-ZNF609 in cardiomyocytes (**Figure 5C**). We then investigated whether the stability of circ-ZNF609 was regulated by RNA m^{6}A methylation. Actinomycin D assay was conducted, and it was found that STM2457 treatment promoted the degradation of circ-ZNF609 in AC16 cardiomyocytes (**Figure 5D**). These data suggest that circ-ZNF609 is negatively regulated by RNA m^{6}A methylation.

Then, we investigated whether the upstream RNA m^{6}A methylation contributes to DOX-induced cardiotoxicity. We first detected the protein expression of RNA methyltransferase METTL3 and METTL14 and found that both were significantly upregulated in DOX-treated mice hearts (Supplemental Figure 6A). METTL3/METTL14 heterodimer comprises the RNA m^{6}A multi-subunit "writer complex"; METTL3 is the enzymatic component whereas METTL14 is an allosteric activator that binds to the target RNA.[26] RNA m^{6}A modification is essential for maintaining cardiac homeostasis. Thus, we first choose to intervene in the expression of METTL14 to achieve a relatively moderately modulation of RNA m^{6}A modification. This positive regulation on circ-ZNF609 was further confirmed by RNA methyltransferase METTL14 knockdown (**Figure 5E**). We then explored the role of METTL14 in DOX-induced cardiotoxicity. METTL14 knockdown was achieved by AAV9-cTnT-shMETTL14 administration via tail vein injection, and after 7 days, DOX was intraperitoneally injected for 5 weeks to establish DOX-induced cardiotoxicity model and the knockdown effect of METTL14 was verified (Supplemental Figure 6B). METTL14 manipulation and DOX treatment presented no alteration on the expression level of linear mRNA *Znf609* and precursor *Znf609* (pre-*Znf609*) (Supplemental Figure 6C). Echocardiographic studies revealed that METTL14 inhibition prevented DOX-treatment induced cardiac dysfunction (EF) and decrease of ventricular anterior wall thickness (LVAWs) (**Figure 5F**). Also, METTL14 knockdown significantly improved DOX-induced cardiomyocyte apoptosis and cardiac fibrosis (**Figure 5G**, Supplemental Figures 6D to 6G). In addition, the decreased protein expression of NRF2 and ABCB8, and the increased protein expression of FTMT were all recovered by METTL14 inhibition in DOX-induced cardiotoxicity (**Figure 5H**). DOX-induced nonheme iron accumulation was also attenuated by METTL14 inhibition in DOX-induced cardiotoxicity, as shown by mitochondria Fe^{3+} detection (**Figure 5I**). Furthermore, the mtDNA copy number which was reduced by DOX treatment was recovered by METTL14 knockdown in the mice hearts (**Figure 5J**). These data show that RNA m^{6}A methylation regulates the stability of circ-ZNF609, and RNA m^{6}A reduction via METTL14 knockdown prevents DOX-induced cardiotoxicity.

THE PROTECTIVE EFFECTS OF METTL14-MEDIATED m^{6}A MODIFICATION IN DOX-INDUCED CARDIOMYOCYTE APOPTOSIS AND OXIDATIVE STRESS ARE DISRUPTED BY CIRC-ZNF609 OVEREXPRESSION. We then further examined the role of METTL14-mediated m^{6}A modification alteration on circ-ZNF609's regulatory effects on DOX-induced cardiomyocyte apoptosis and oxidative stress. METTL14 inhibition decreased the total RNA m^{6}A methylation (**Figure 6A**). The protective effects of METTL14 knockdown were shown by alleviated TUNEL staining and mitochondria ROS accumulation (**Figures 6B and 6C**). Next, we cotransfected circ-ZNF609 overexpression (circ-ZNF609 OE)

FIGURE 6 Continued

(A) Decreased total RNA m^{6}A methylation level in the NRCM treated with shMETTL14 (**$P < 0.01$, n = 6 wells/group). **(B)** Representative images of immunofluorescence staining and quantification of the TUNEL-positive cardiomyocytes displayed the protective effect of METTL14 knockdown on cardiomyocytes apoptosis in DOX-treated NRCM (**$P < 0.01$, n = 6 wells/group, scale bar = 100 μm). **(C)** Representative images of immunofluorescence staining and quantification of the mitochondrial ROS level displayed the protective effect of METTL14 knockdown on oxidative stress in DOX-treated NRCM (**$P < 0.01$, n = 50 cardiomyocytes/group, scale bar = 20 μm). **(D)** Representative images of immunofluorescence staining and quantification of the TUNEL-positive cardiomyocytes displayed the disrupt effect of circ-ZNF609 overexpression on METTL14 knockdown in DOX-treated NRCM (**$P < 0.01$, n = 6 wells/group, scale bar = 100 μm). **(E)** Western blot analysis of Bax and Bcl-2 revealed the blocked antiapoptosis effect of circ-ZNF609 overexpression on METTL14 knockdown in the DOX-treated NRCM (**$P < 0.01$, n = 6 wells/group). **(F)** Representative images of immunofluorescence staining and quantification of the mitochondrial ROS level displayed the block effect of circ-ZNF609 overexpression on METTL14 knockdown in DOX-treated NRCM (**$P < 0.01$, n = 50 cardiomyocytes/group, scale bar = 20 μm). **(G)** Quantification of intracellular ROS levels revealed the block effect of circ-ZNF609 overexpression on METTL14 knockdown in DOX-treated NRCM, as evidenced by DHE staining (**$P < 0.01$, n = 6 wells/group). **(H)** Western blot analysis of NRF2, ABCB8, and FTMT revealed the block effect of circ-ZNF609 overexpression on METTL14 knockdown in DOX-treated NRCM (*$P < 0.05$, **$P < 0.01$, n = 3 wells/group). **(I)** The analysis of mitochondrial DNA level revealed the block effect of circ-ZNF609 overexpression on METTL14 knockdown in DOX-treated NRCM (**$P < 0.01$, n = 6 wells/group). All data are expressed as mean ± SD. (**A**, Student *t* test. **B**, 2-way ANOVA with Tukey's post hoc test. **C**, Kruskal-Wallis test. **D to I**, 2-way ANOVA with Tukey's post hoc test.) Abbreviations as in **Figures 1 to 3**.

FIGURE 7 The Early Application of circ-ZNF609 Suppression Has Therapeutic Effects on the DOX-Induced Cardiotoxicity

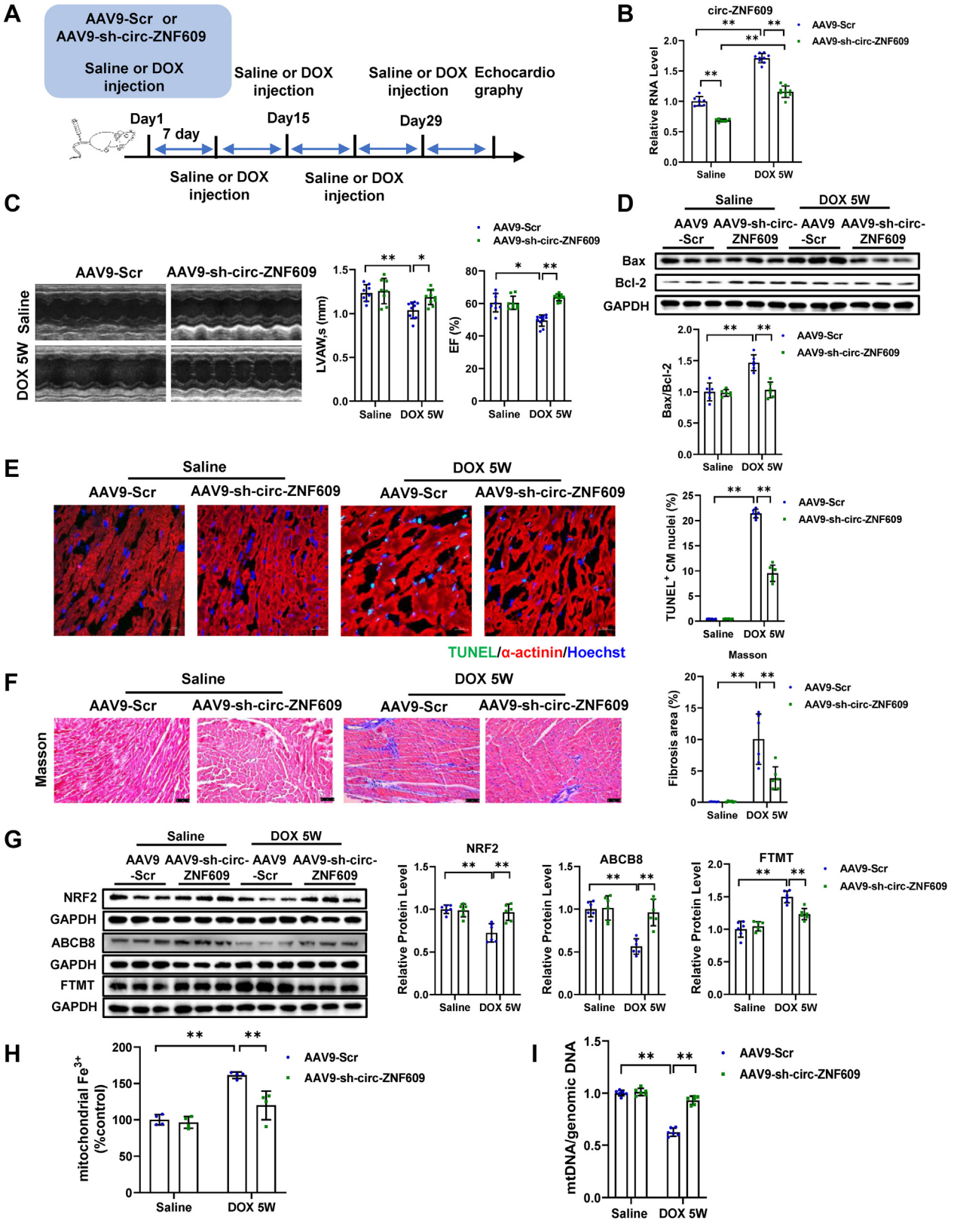

Continued on the next page

and METTL14 knockdown (METTL14 shRNA) constructs and examined cardiomyocyte apoptosis and oxidative stress production. As shown in **Figures 6D and 6E**, TUNEL staining and Bax/Bcl-2 ratio showed that overexpression of circ-ZNF609 blocked the antiapoptotic effect of METTL14 knockdown in NRCMs. We then measured the level of oxidative stress in NRCMs and found that the reduction effect of METTL14 suppression on ROS production was reversed by circ-ZNF609 overexpression as evaluated by MitoSOX staining and DHE staining (**Figures 6F and 6G**). In addition, western blot detection of NRF2, FTMT, and ABCB8 also showed that the effects of METTL14 shRNA in regulating the expression of those proteins were blunted by circ-ZNF609 (**Figure 6H**). Moreover, overexpression of circ-ZNF609 abolished the protective effects of METTL14 knockdown on mitochondrial DNA content (**Figure 6I**). In summary, those data show that the protective effects of METTL14 inhibition on DOX-induced cardiomyocyte apoptosis and oxidative stress are disrupted by circ-ZNF609 overexpression.

THE EARLY APPLICATION OF CIRC-ZNF609 SUPPRESSION HAS THERAPEUTIC EFFECTS ON THE DOX-INDUCED CARDIOTOXICITY. To investigate the clinical application of circ-ZNF609 as a biological therapy, we simulated the situation by injecting AAV9 at the same day after DOX administration to build an early phase therapeutic model on DOX-induced cardiotoxicity (**Figure 7A**). The knockdown effect of AAV9-sh-circ-ZNF609 was verified by qRT-PCR (**Figure 7B**). As measured by echocardiography, we found that circ-ZNF609 knockdown improved cardiac function and ventricular wall thickness as suggested by improved EF and LVAWs (**Figure 7C**). Next, we assessed the cardiac apoptosis and fibrosis in DOX-induced cardiotoxicity. As shown in **Figures 7D and 7E**, Bax/Bcl-2 ratio and TUNEL staining showed that AAV9-sh-circ-ZNF609 administration significantly reduced DOX-induced apoptosis. In addition, Masson staining and Sirius red staining suggested that cardiac fibrosis was attenuated by circ-ZNF609 knockdown in the DOX-treatment group (**Figure 7F**, Supplemental Figure 7A). Consistently, the expression of fibrotic genes (*Col1a1*, *Col3a1*, and *α-Sma*) was decreased after AAV9-sh-circ-ZNF609 administration (Supplemental Figure 7B). In addition, the decreased protein expression of NRF2 and ABCB8, and the increased protein expression of FTMT were all recovered by circ-ZNF609 knockdown in DOX-induced cardiotoxicity (**Figure 7G**). DOX-induced nonheme iron accumulation was also attenuated by circ-ZNF609 knockdown in DOX-induced cardiotoxicity, as shown by mitochondria Fe^{3+} detection (**Figure 7H**). Furthermore, the mtDNA copy number which was reduced by DOX treatment was recovered by circ-ZNF609 knockdown in the mice hearts (**Figure 7I**). Collectively, our results show that circ-ZNF609 knockdown can be an effective therapeutic strategy against DOX-induced cardiotoxicity.

DISCUSSION

Recent studies on the mechanism of DOX-induced cardiotoxicity have attracted vast interest from the scientific community worldwide, while research on the roles of circRNAs in DOX-induced cardiotoxicity is still in its infancy. Here, we found that circ-ZNF609 was upregulated in adult mouse cardiomyocytes in response to DOX-induced cardiotoxicity. Knockdown of circ-ZNF609 in cardiomyocytes demonstrated cardioprotective and therapeutic effects against DOX-induced cardiomyocyte toxicity both in vivo and in vitro. Mechanistically, circ-ZNF609 knockdown alleviated DOX-induced cardiotoxicity through attenuating cardiomyocyte apoptosis, reducing ROS accumulation, and ameliorating the mitochondrial iron overload. circ-ZNF609 inhibition could block the effects that elevation of RNA m^6A methylation levels exert on mice hearts after DOX treatment, whereas

FIGURE 7 Continued

(A) The schedule of therapeutic experiment based on AAV9-sh-circ-ZNF609 virus injection and DOX-induced mice cardiotoxicity model establishment. **(B)** Knockdown effects of AAV9-sh-circ-ZNF609 in the mice hearts, as evidenced by qRT-PCR (**$P < 0.01$, n = 7:7:9:9 mice, respectively). **(C)** Improved left ventricular EF and LVAWs in the DOX-induced cardiotoxicity mice hearts after treated with AAV9-sh-circ-ZNF609 for therapy, as evidenced by echocardiography (*$P < 0.05$, **$P < 0.01$, n = 8:8:10:10 mice, respectively). **(D)** Western blot analysis of Bax and Bcl-2 in the DOX-induced cardiotoxicity mice hearts after injected with or without AAV9-sh-circ-ZNF609 for therapy (**$P < 0.01$, n = 6 mice/group). **(E)** Attenuated myocardial apoptosis in the DOX-induced cardiotoxicity mice hearts after treated with AAV9-sh-circ-ZNF609 for therapy, as evidenced by TUNEL staining (**$P < 0.01$, n = 6 mice/group, scale bar = 20 μm). **(F)** Reduced cardiac fibrosis in the DOX-induced cardiotoxicity mice hearts after treated with AAV9-sh-circ-ZNF609 for therapy, as evidenced by Masson's staining (**$P < 0.01$, n = 6 mice/group, scale bar = 50 μm). **(G)** Western blot analysis of NRF2, ABCB8, and FTMT in the DOX-induced cardiotoxicity mice hearts after injected with or without AAV9-sh-circ-ZNF609 for therapy (**$P < 0.01$, n = 6 mice/group). **(H)** Mitochondrial nonheme iron (Fe^{3+}) in the DOX-induced cardiotoxicity mice hearts after injected with or without AAV9-sh-circ-ZNF609 for therapy (**$P < 0.01$, n = 4 mice/group). **(I)** The mitochondrial DNA levels in the DOX-induced cardiotoxicity mice hearts after treated with or without AAV9-sh-circ-ZNF609 for therapy (**$P<0.01$, n = 6 mice/group). Data are presented as mean ± SD. (**B**, 2-way ANOVA with Tukey's post hoc test. **C**, Left: 2-way ANOVA with Tukey's post hoc test, **right**: Kruskal-Wallis test. **D to I**, 2-way ANOVA with Tukey's post hoc test.) Abbreviations as in **Figures 1 to 3**.

FIGURE 8 Proposed Working Model by Which Downregulation of circ-ZNF609 Protects Against DOX-Induced Cardiotoxicity

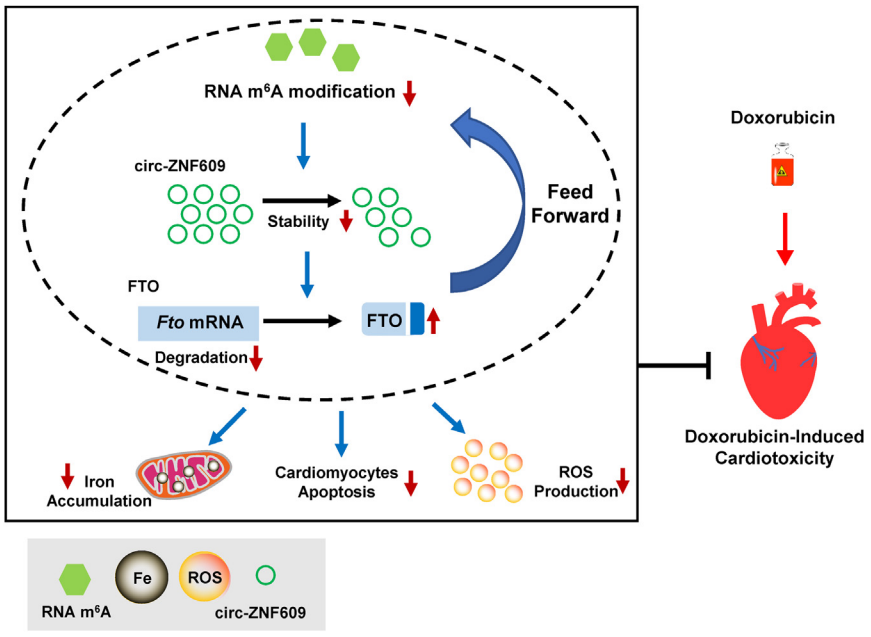

circ-ZNF609 is upregulated via RNA m^{6}A methylation in response to DOX treatment. Mechanistically, circ-ZNF609 knockdown alleviates DOX-induced cardiotoxicity through attenuating cardiomyocyte apoptosis, reducing ROS accumulation and ameliorating the mitochondrial iron overload. circ-ZNF609 knockdown can be protective against DOX-induced cardiotoxicity via inhibiting the degradation of *Fto*. Abbreviations as in Figures 1 to 3.

RNA m^{6}A demethylase FTO acted as the downstream factor of circ-ZNF609 in response to DOX stimulation. Moreover, the stability of circ-ZNF609 was regulated by RNA m^{6}A methylation, and suppression of RNA m^{6}A methylation by METTL14 modulated the function of circ-ZNF609 in DOX-induced cardiotoxicity. Our study uncovers that circ-ZNF609 may act as a bridge to mediate the regulation between m^{6}A effectors, expanding the fundamental role of circRNAs (**Figure 8**).

A major challenge in the field of cardio-oncology has been to maintain a balance between the survival benefits and cardiotoxicity deficits of current treatment protocols. The function of circ-ZNF609 knockdown in tumor cells is reported to have treatment benefits for a multitude of cancers.[27-30] In addition, silencing of circ-ZNF609 could increase the sensitivity of prostate cancer cells to radiotherapy in vivo.[31] In the present study, although the fold change of circ-ZNF609 regulation in the heart is at a moderate level, we found that downregulation of circ-ZNF609 conferred resistance to chemotherapy-induced toxicity of chemotherapy in cardiomyocytes, of which functions is also protective to the hearts. Previously, we have shown that circ-ZNF609 is abundantly expressed in primary neonatal rat cardiomyocytes and less expressed in neonatal rat cardiac fibroblasts.[11] Here, we suggest that circ-ZNF609 is more abundant in adult mouse cardiomyocytes than adult mouse cardiac fibroblasts (Supplemental Figure 8A). Also, we observe that DOX-treatment significantly elevates the expression of circ-ZNF609 (~ 2-fold) in cardiomyocytes but has no obvious effect on isolated cardiac fibroblasts (Supplemental Figure 8B). Thus, the fold-change of circ-ZNF609 in cardiomyocytes might be responsible for the mildly increased levels of circ-ZNF609 in the whole heart during DOX-induced cardiotoxicity. To further confirm whether the observed effects derive mainly from cardiomyocytes, we characterized cardiomyocytes specific changes and infection rates of AAV9 in isolated adult mouse cardiomyocytes in RNA expression with sh-circ-ZNF609 AAV9 or its control virus injection. The verified infection rate of AAV9 showed that ~ 40% to 60% AAV9 through tail-vein injection can effectively infect adult mouse cardiomyocytes, consistent with the RNA level expression change of circ-ZNF609 in isolated adult mouse cardiomyocytes (Supplemental Figures 8C and 8D). These data suggest that the specific changes and

infection rates of AAV9-sh-circ-ZNF609 injection on cardiomyocytes (~0.4- to 0.6-fold reduction) were comparable to the fold-change of circ-ZNF609 RNA expression level in DOX-treated adult mouse cardiomyocytes (~ 2-fold increase). This, in turn, may indicate the important role of circ-ZNF609 in cardiomyocyte in DOX-induced cardiotoxicity and explain why pronounced phenotypic effects are produced by relatively small changes in expression levels. Moreover, to investigate the therapeutic potential and utility of circ-ZNF609, we silenced circ-ZNF609 by injecting AAV9 at the same day after DOX administration to build an early phase therapeutic strategy against DOX-induced cardiotoxicity, which confirmed the therapeutic effects of circ-ZNF609 knockdown. Taken together, our data suggest that even moderate fluctuations in the levels of circ-ZNF609 in cardiomyocytes may exert an important role in DOX-induced cardiotoxicity. In turn, this may also provide an opportunity for developing new anticancer treatment protocols which could promote the efficacy of chemotherapy on tumor tissues while attenuating the cardiotoxicity of chemotherapy.

RNA m^{6}A modification is the most common internal modification of RNA.[32] It is a dynamic and reversible process, which can be regulated by m^{6}A methyltransferases, demethylases, and m^{6}A-binding proteins.[33] RNA m^{6}A methylation has been reported to be a key player not only in maintaining cardiovascular homeostasis but also in the pathogenesis of cardiovascular diseases.[17,23,34-36] RNA methyltransferase METTL3 was found to be involved in the regulation of cardiac hypertrophy and cardiomyocyte autophagy.[34,37,38] Furthermore, studies on murine models show that demethylase FTO levels were significantly decreased in cardiac tissue with heart failure, and upregulation of FTO in the heart of mice can significantly inhibit both ischemic and pressure overload-induced heart failure.[17,23] However, the role of FTO as well as RNA m^{6}A modification (both associated with circRNA) in regulating DOX-induced cardiotoxicity remains unknown. Here, we found that circ-ZNF609 overexpression abrogated the protective effects of METTL14 knockdown, whereas FTO inhibition abolished the protective effects of circ-ZNF609 knockdown in DOX-induced cardiotoxicity, showing the important function of circRNA as well as m^{6}A modification in DOX-induced cardiotoxicity. However, FTO or METTL14 alteration does not affect the mitochondrial ROS generation or protein expression related to iron homeostasis under basal conditions. Further, we examined the expression of NRF2, FTMT, and ABCB8 by using FTO inhibitor FB23-2 and m^{6}A inhibitor STM2457 with or without DOX-treatment. Our data indicate that STM2457 treatment exhibits recovery effects on the expression of NRF2, FTMT, and ABCB8 under the stimulation of DOX, whereas FB23-2 exert further deterioration on those proteins (Supplemental Figures 9A and 9B). Similar results are obtained by MitoSOX staining after using FB23-2 and STM2457 treatment (Supplemental Figures 9C and 9D). Furthermore, STM2457 treatment was shown to reduce the mitochondrial ROS content in response to DOX whereas circ-ZNF609 overexpression blunted these protective effects. On the contrary, FB23-2 treatment was found to disrupt the attenuation of DOX-induced mitochondrial ROS generation after circ-ZNF609 knockdown (Supplemental Figures 9C and 9D). These data indicate that changes of mitochondrial ROS regulators and iron homeostasis in DOX-treated cardiomyocytes are regulated indirectly through m^{6}A modification by circ-ZNF609. Further investigation including MeRIP-sequencing is warranted to elucidate the global RNA m^{6}A methylation alteration pattern in response to DOX-induced cardiotoxicity and identify the direct targets of FTO to provide significant understanding of post-transcriptional regulation mechanisms in the DOX-treated heart. The interplay between RNA m^{6}A writer and eraser has been observed previously in cancer progression.[39] However, the underlying mechanism of cross-talk between m^{6}A writer and eraser remains to be elucidated. In the present study, we found that, circ-ZNF609 which was regulated by RNA m^{6}A methylation, regulates, in turn, the expression of m^{6}A demethylase FTO. Thus, our study here uncovers an additional key role for circRNA that may act as a bridge to mediate the regulation between m^{6}A effectors, expanding the intracellular fundamental functional role of circRNAs.

ROS production is one of the main features of DOX-induced cardiotoxicity.[7,40] DOX could affect ROS metabolism in cellular level through several paths, including damage of cardiolipin, disruption of cellular iron metabolism, and perturbation of cellular respiratory chain mediated by nicotinamide adenine dinucleotide phosphate.[19,21,41,42] A previous study reported that circRNA circITCH could act as miR-330-5p sponge to regulate ROS production via SITR6 in DOX-induced cardiotoxicity.[43] In addition to SIRT6, many other factors have also been identified as part of the physiologic response to oxidative stress and ROS generation. However, whether circRNAs participate in those processes remains largely unknown. Transcription factor NRF2 serves as a crucial regulator of intracellular antioxidant response.[44] Here, we found

that circ-ZNF609 inhibition in DOX-treated cardiomyocytes significantly recovered the expression level of NRF2, and restored the intracellular and mitochondrial ROS levels. Previous studies have shown that DOX treatment could cause deletion or point mutation in the "hot spot" region of mitochondrial DNA, thus leading to abnormal replication and early degradation.[45] Increased levels of mitochondrial ROS content are shown to further cause mtDNA depletion, accumulation of oxidized proteins and lipids, and decreased mitochondrial respiration efficiency.[46] In the present study, knockdown of circ-ZNF609 alleviated the iron accumulation and mtDNA copy number depletion caused by DOX treatment, as evidenced by decreased intracellular iron, increased ABCB8 protein, reduced expression of mitochondrial iron storage protein FTMT, and increased mtDNA copy number. The observed mtDNA content recovery after circ-ZNF609 suppression might reflect a DNA damage alleviation pathway. Other mechanisms that may be or may be not related to circ-ZNF609 could also be contributing to the mtDNA content changes as well as the ameliorated DOX-induced cardiotoxicity. Iron accumulation in mitochondria is another important factor implicated in states of increased lipid peroxidation and intracellular ROS levels.[47-49] ABCB8, which is the main regulator of ferritin transport in mitochondria, was shown to be involved in the maturation of cytosolic Fe/S proteins and protects the heart from oxidative stress.[50] Thus, our data indicate that circ-ZNF609 suppression could attenuate DOX-induced cardiotoxicity by alleviating iron overload, mtDNA copy number depletion, and reduction in ROS generation. In summary, our study explored the regulatory function of circ-ZNF609 on mitochondrial ROS production in DOX-induced cardiotoxicity, which might also represent a promising potential therapeutic target for incorporation into antioxidant treatment protocols protecting against DOX-induced cardiotoxicity.

STUDY LIMITATIONS. Our study shows that circ-ZNF609, which is regulated by RNA m^6A methylation, in turn, modulates the expression m^6A demethylase FTO, and circ-ZNF609 inhibition exhibits protective and therapeutic effects on DOX-induced cardiotoxicity. However, the detailed mechanism of m^6A modification in regulating DOX-induced cardiotoxicity is not deeply explored in this study and needs further investigation. Future studies designed to answer fundamental questions about the underlying regulatory mechanism of RNA m^6A methylation alteration in response to DOX-induced cardiotoxicity would offer significant opportunity for further elucidating the biological role of RNA m^6A as well as developing DOX-induced cardiotoxicity therapeutic protocols. Although RNA and protein levels of FTO are both negatively regulated by circ-ZNF609, in present study, circ-ZNF609 alteration did not demonstrate much of changes related to cardiomyocytes apoptosis and oxidative stress under non-DOX treatment conditions. This indicate that other downstream factors or signaling pathways within cardiomyocytes might be involved in the regulating functions of circ-ZNF609. Further studies focus on the mechanism of circ-ZNF609 on cardiomyocytes at the basal condition would provide more information about the fundamental understanding about circ-ZNF609. Moreover, our study shows the protective effects of circ-ZNF609 on DOX-induced cardiotoxicity in tumor-free animals, but whether it would affect the efficacy of DOX as a chemotherapeutic agent for tumors remains unknown. Considering that circ-ZNF609 was found to be upregulated in a variety of tumor cells, targeting circ-ZNF609 might simultaneously have an impact on tumor growth. Thus, whether circ-ZNF609 inhibition could achieve a dual therapeutic benefit in cancer therapy by simultaneously preventing DOX-induced cardiotoxicity and reducing tumor growth warrants further investigation.

CONCLUSIONS

Our study reveals that circ-ZNF609 is upregulated via RNA m^6A methylation in response to DOX treatment. circ-ZNF609 knockdown has been shown to be protective against DOX-induced cardiotoxicity via inhibiting the degradation of *Fto*, exhibiting promising potential for novel therapy development.

FUNDING SUPPORT AND AUTHOR DISCLOSURES

This work was supported by the grants from National Key Research and Development Project (2018YFE0113500 to Dr Xiao), National Natural Science Foundation of China (82020108002 and 82225005 to Dr Xiao, 82270291 to Dr Wang), Innovation Program of Shanghai Municipal Education Commission (2017-01-07-00-09-E00042 to Dr Xiao), the grant from Science and Technology Commission of Shanghai Municipality (21XD1421300 and 20DZ2255400 to Dr Xiao), and the "Dawn" Program of Shanghai Education Commission (19SG34 to Dr Xiao). All other authors have reported that they have no relationships relevant to the contents of this paper to disclose.

ADDRESS FOR CORRESPONDENCE: Dr Junjie Xiao or Dr Lijun Wang, Institute of Cardiovascular Sciences, Shanghai Engineering Research Center of Organ Repair, School of Life Science, Shanghai University, 333 Nan Chen Road, Shanghai 200444, China. E-mail: junjiexiao@shu.edu.cn OR lijunwang@shu.edu.cn.

PERSPECTIVES

COMPETENCY IN MEDICAL KNOWLEDGE: The cardiotoxicity resulting from chemotherapy has been proven to pose a significant risk for cancer patients. Balancing survival benefits with cardiotoxic drawbacks has been a major challenge in the field of cardio-oncology. However, there are still no effective therapies against DOX-induced cardiotoxicity. circ-ZNF609 knockdown has been reported to exert suppressive effects on the growth rate of many cancers, whereas the function of circ-ZNF609 in the cardiovascular disease caused by anticancer treatment remains unknown.

TRANSLATIONAL OUTLOOK: Knockdown of circ-ZNF609 can attenuate DOX-induced cardiotoxicity by decreasing ROS production and mitochondrial iron accumulation, suggesting that circ-ZNF609 could be used as a potential therapeutic target for DOX-induced cardiotoxicity. The findings of this study may provide an opportunity for developing new anticancer approach which could promote the efficacy of chemotherapy on tumor tissues while attenuating the cardiotoxicity of chemotherapy.

REFERENCES

1. Livshits Z, Rao RB, Smith SW. An approach to chemotherapy-associated toxicity. *Emerg Med Clin North Am*. 2014;32:167–203.

2. Rochette L, Guenancia C, Gudjoncik A, et al. Anthracyclines/trastuzumab: new aspects of cardiotoxicity and molecular mechanisms. *Trends Pharmacol Sci*. 2015;36:326–348.

3. Herrmann J. Adverse cardiac effects of cancer therapies: cardiotoxicity and arrhythmia. *Nat Rev Cardiol*. 2020;17:474–502.

4. Bartlett JJ, Trivedi PC, Pulinilkunnil T. Autophagic dysregulation in doxorubicin cardiomyopathy. *J Mol Cell Cardiol*. 2017;104:1–8.

5. Mizutani H, Tada-Oikawa S, Hiraku Y, Kojima M, Kawanishi S. Mechanism of apoptosis induced by doxorubicin through the generation of hydrogen peroxide. *Life Sci*. 2005;76:1439–1453.

6. Kalyanaraman B, Joseph J, Kalivendi S, Wang S, Konorev E, Kotamraju S. Doxorubicin-induced apoptosis: implications in cardiotoxicity. *Mol Cell Biochem*. 2002;234-235:119–124.

7. Songbo M, Lang H, Xinyong C, Bin X, Ping Z, Liang S. Oxidative stress injury in doxorubicin-induced cardiotoxicity. *Toxicol Lett*. 2019;307:41–48.

8. Christidi E, Brunham LR. Regulated cell death pathways in doxorubicin-induced cardiotoxicity. *Cell Death Dis*. 2021;12:339.

9. Memczak S, Jens M, Elefsinioti A, et al. Circular RNAs are a large class of animal RNAs with regulatory potency. *Nature*. 2013;495:333–338.

10. Chen LL. The expanding regulatory mechanisms and cellular functions of circular RNAs. *Nat Rev Mol Cell Biol*. 2020;21:475–490.

11. Wang L, Yu P, Wang J, et al. Downregulation of circ-ZNF609 promotes heart repair by modulating RNA N^6-methyladenosine-modified *Yap* expression. *Research (Wash D C)*. 2022;2022:9825916.

12. Salgado-Somoza A, Zhang L, Vausort M, Devaux Y. The circular RNA MICRA for risk stratification after myocardial infarction. *Int J Cardiol Heart Vasc*. 2017;17:33–36.

13. Vausort M, Salgado-Somoza A, Zhang L, et al. Myocardial infarction-associated circular RNA predicting left ventricular dysfunction. *J Am Coll Cardiol*. 2016;68:1247–1248.

14. Wang S, Xue X, Wang R, et al. CircZNF609 promotes breast cancer cell growth, migration, and invasion by elevating p70S6K1 via sponging miR-145-5p. *Cancer Manag Res*. 2018;10:3881–3890.

15. Wu X, Wang L, Wang K, et al. ADAR2 increases in exercised heart and protects against myocardial infarction and doxorubicin-induced cardiotoxicity. *Mol Ther*. 2022;30:400–414.

16. Liu J, Eckert MA, Harada BT, et al. m(6)A mRNA methylation regulates AKT activity to promote the proliferation and tumorigenicity of endometrial cancer. *Nat Cell Biol*. 2018;20:1074–1083.

17. Zhang B, Jiang H, Wu J, et al. m6A demethylase FTO attenuates cardiac dysfunction by regulating glucose uptake and glycolysis in mice with pressure overload-induced heart failure. *Signal Transduct Target Ther*. 2021;6:377.

18. Li J, Chan MC, Yu Y, et al. miR-29b contributes to multiple types of muscle atrophy. *Nat Commun*. 2017;8:15201.

19. Li S, Wang W, Niu T, et al. Nrf2 deficiency exaggerates doxorubicin-induced cardiotoxicity and cardiac dysfunction. *Oxid Med Cell Longev*. 2014;2014:748524.

20. Wallace KB, Sardao VA, Oliveira PJ. Mitochondrial determinants of doxorubicin-induced cardiomyopathy. *Circ Res*. 2020;126:926–941.

21. Ichikawa Y, Ghanefar M, Bayeva M, et al. Cardiotoxicity of doxorubicin is mediated through mitochondrial iron accumulation. *J Clin Invest*. 2014;124:617–630.

22. Fang X, Wang H, Han D, et al. Ferroptosis as a target for protection against cardiomyopathy. *Proc Natl Acad Sci U S A*. 2019;116:2672–2680.

23. Mathiyalagan P, Adamiak M, Mayourian J, et al. FTO-Dependent m6A regulates cardiac function during remodeling and repair. *Circulation*. 2019;139:518–532.

24. Di Timoteo G, Dattilo D, Centron-Broco A, et al. Modulation of circRNA metabolism by m(6)A modification. *Cell Rep*. 2020;31:107641.

25. Yankova E, Blackaby W, Albertella M, et al. Small-molecule inhibition of METTL3 as a strategy against myeloid leukaemia. *Nature*. 2021;593:597–601.

26. Wang X, Feng J, Xue Y, et al. Structural basis of N(6)-adenosine methylation by the METTL3-METTL14 complex. *Nature*. 2016;534:575–578.

27. Qian Y, Li Y, Li R, Yang T, Jia R, Ge YZ. circ-ZNF609: a potent circRNA in human cancers. *J Cell Mol Med*. 2021;25:10349–10361.

28. Liu Z, Pan HM, Xin L, et al. Circ-ZNF609 promotes carcinogenesis of gastric cancer cells by inhibiting miRNA-145-5p expression. *Eur Rev Med Pharmacol Sci*. 2019;23:9411–9417.

29. Wu L, Xia J, Yang J, et al. Circ-ZNF609 promotes migration of colorectal cancer by inhibiting Gli1 expression via microRNA-150. *J BUON*. 2018;23:1343–1349.

30. Zuo Y, Shen W, Wang C, Niu N, Pu J. Circular RNA circ-ZNF609 promotes lung adenocarcinoma proliferation by modulating miR-1224-3p/ETV1 signaling. *Cancer Manag Res*. 2020;12:2471–2479.

31. Du S, Zhang P, Ren W, Yang F, Du C. Circ-ZNF609 accelerates the radioresistance of prostate cancer cells by promoting the glycolytic metabolism through miR-501-3p/HK2 axis. *Cancer Manag Res*. 2020;12:7487–7499.

32. Jiang X, Liu B, Nie Z, et al. The role of m6A modification in the biological functions and diseases. *Signal Transduct Target Ther*. 2021;6:74.

33. Yang Y, Hsu PJ, Chen YS, Yang YG. Dynamic transcriptomic m(6)A decoration: writers, erasers, readers and functions in RNA metabolism. *Cell Res*. 2018;28:616–624.

34. Dorn LE, Lasman L, Chen J, et al. The m(6)A mRNA methylase METTL3 controls cardiac homeostasis and hypertrophy. *Circulation*. 2019;139:533–545.

35. Berulava T, Buchholz E, Elerdashvili V, et al. Changes in m6A RNA methylation contribute to heart failure progression by modulating translation. *Eur J Heart Fail*. 2020;22:54–66.

36. Wang L, Wang J, Yu P, et al. METTL14 is required for exercise-induced cardiac hypertrophy and protects against myocardial ischemia-reperfusion injury. *Nat Commun*. 2022;13:6762.

37. Song H, Feng X, Zhang H, et al. METTL3 and ALKBH5 oppositely regulate m(6)A modification of TFEB mRNA, which dictates the fate of hypoxia/reoxygenation-treated cardiomyocytes. *Autophagy*. 2019:1–19.

38. Gao XQ, Zhang YH, Liu F, et al. The piRNA CHAPIR regulates cardiac hypertrophy by controlling METTL3-dependent N(6)-methyladenosine methylation of Parp10 mRNA. *Nat Cell Biol*. 2020;22:1319–1331.

39. Panneerdoss S, Eedunuri VK, Yadav P, et al. Cross-talk among writers, readers, and erasers of m(6)A regulates cancer growth and progression. *Sci Adv*. 2018;4:eaar8263.

40. Donato C, Antonella DA, Luigi S, et al. Oxidative stress and cellular response to doxorubicin: a common factor in the complex milieu of anthracycline cardiotoxicity. *Oxid Med Cell Longev*. 2017;2017:1521020.

41. Ma Cca Rinelli F, Gammella E, Asperti M, et al. Mice lacking mitochondrial ferritin are more sensitive to doxorubicin-mediated cardiotoxicity. *J Mol Med*. 2014;92:859–869.

42. Goormaghtigh E, Huart P, Praet M, Brasseur R, Ruysschaert JM. Structure of the adriamycin-cardiolipin complex. Role in mitochondrial toxicity. *Biophys Chem*. 1990;35:247–257.

43. Han D, Wang Y, Wang Y, et al. The tumor-suppressive human circular RNA CircITCH sponges miR-330-5p to ameliorate doxorubicin-induced cardiotoxicity through upregulating SIRT6, survivin, and SERCA2a. *Circ Res*. 2020;127:e108–e125.

44. Kovac S, Angelova PR, Holmström KM, Zhang Y, Dinkova-Kostova AT, Abramov AY. Nrf2 regulates ROS production by mitochondria and NADPH oxidase. *Biochim Biophys Acta*. 2015;1850:794–801.

45. Lebrecht D, Setzer B, Ketelsen UP, Haberstroh J, Walker UA. Time-dependent and tissue-specific accumulation of mtDNA and respiratory chain defects in chronic doxorubicin cardiomyopathy. *Circulation*. 2003;108:2423–2429.

46. Quan Y, Xin Y, Tian G, Zhou J, Liu X. Mitochondrial ROS-modulated mtDNA: a potential target for cardiac aging. *Oxid Med Cell Longev*. 2020;2020:9423593.

47. Galaris D, Barbouti A, Pantopoulos K. Iron homeostasis and oxidative stress: an intimate relationship. *Biochim Biophys Acta Mol Cell Res*. 2019;1866:118535.

48. Mancardi D, Mezzanotte M, Arrigo E, Barinotti A, Roetto A. Iron overload, oxidative stress, and ferroptosis in the failing heart and liver. *Antioxidants (Basel)*. 2021;10.

49. Read AD, Bentley RE, Archer SL, Dunham-Snary KJ. Mitochondrial iron-sulfur clusters: structure, function, and an emerging role in vascular biology. *Redox Biol*. 2021;47:102164.

50. Liesa M, Qiu W, Shirihai OS. Mitochondrial ABC transporters function: the role of ABCB10 (ABC-me) as a novel player in cellular handling of reactive oxygen species. *Biochim Biophys Acta*. 2012;1823:1945–1957.

KEY WORDS circ-ZNF609, doxorubicin-induced, circular RNA, cardiotoxicity, RNA N^6-methyladenosine

APPENDIX For supplemental figures and tables, please see the online version of this paper.